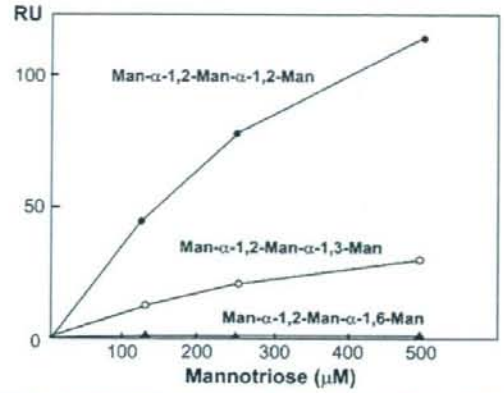

FIGURE 4. **Specific binding of GST-VIP36 to the D1 arm (Man-α-1,2-Man-α-1,2-Man) revealed by SPR analysis.** Three different mannotrioses were added over flow cells at the indicated concentrations. Specific binding of mannotrioses was obtained by subtracting the resonance unit (*RU*) value of the GST immobilized sensor chip from the values of GST-VIP36 immobilized sensor chips. The plots were obtained by subtracting the values measured using the sample buffer without carbohydrates. The dose binding curves were obtained from the resonance unit value at 200 s. *Solid circle*, Man-α-1,2-Man-α-1,2-Man; *open circle*, Man-α-1,2-Man-α-1,3-Man; *solid triangle*, Man-α-1,2-Man-α-1,6-Man.

respectively (Fig. 5*E*). In contrast, the hydrogen bond between the 6-OH group and Asp^{261} (Oδ-1) is not observed in molecule B (supplemental Fig. 4A). The binding site of the reducing-end mannose residue of Man_2 is almost the same as the primary binding site (Fig. 5, *D* and *E*).

Structure of VIP36 in Complex with Ca^{2+} and $Man_3GlcNAc$—In the structure of VIP36 with $Man_3GlcNAc$, the Man_3 moiety is ordered, whereas the GlcNAc moiety is disordered. The Man-α-1,2-Man-α-1,3-Man residues have defined electron density (Fig. 5*C*). The binding site of the non-reducing mannose residue of $Man_3GlcNAc$ is almost the same as the primary binding site (Fig. 5, *D* and *F*). The 6-OH group of the α1–2- and α1–3-linked mannose residue makes hydrogen bonds with Tyr^{164} (Oη) and Asn^{166} (O) (Fig. 5*F*). The α1–3- and β1–4-linked mannose residue is recognized by Asp^{261} (Oδ-1) through a hydrogen bond, whereas the hydrogen bond is not observed in molecule B (supplemental Fig. 4B).

DISCUSSION

Many lectins, such as mannose-binding proteins and the asialoglycoprotein receptors, achieve higher affinity and selectivity through oligomerization of their CRDs (43). For instance, ERGIC-53 and Emp46/47p are known to form oligomeric complexes through the putative coiled-coil region in the stalk domain (15, 44, 45). On the other hand, it has been shown that

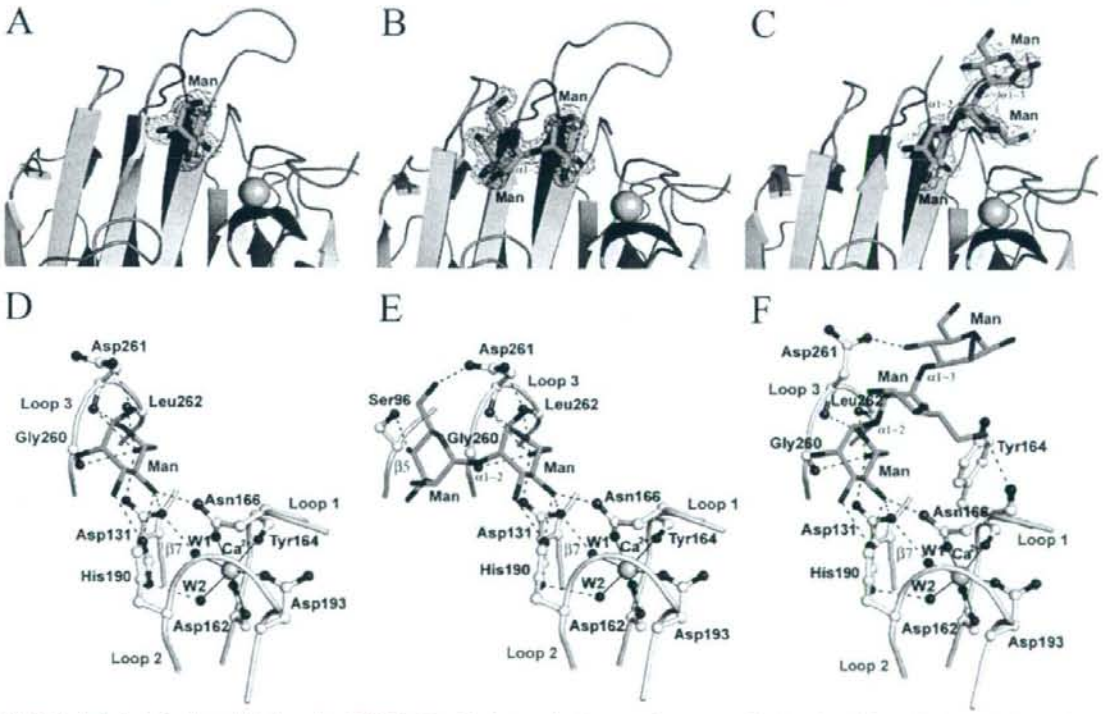

FIGURE 5. **Carbohydrate ligand-binding site of VIP36.** $2F_o - F_c$ electron density map of mannose of the Man-bound form (*A*), Man-α-1,2-Man of the Man_2-bound form (*B*), and Man-α-1,2-Man-α-1,3-Man of the $Man_3GlcNAc$-bound form (*C*) contoured at 1.2σ. Secondary structures are shown as in Fig. 2*A*. *D*, structure of mannose and Ca^{2+}-binding site of VIP36 (molecule A). *E*, structure of Man-α-1,2-Man and Ca^{2+}-binding site of VIP36 (molecule A). *F*, structure of Man-α-1,2-Man-α-1,3-Man and Ca^{2+}-binding site of VIP36 (molecule A). The bound carbohydrate residues are shown as *green stick* models. Residues of VIP36 binding to the ligands are shown in *ball-and-stick* models.

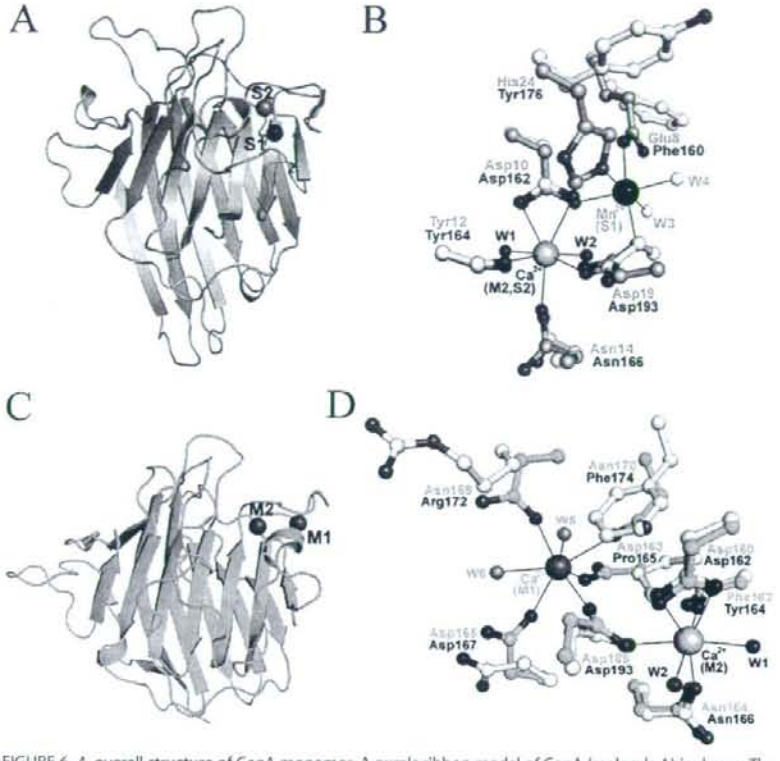

FIGURE 6. *A*, overall structure of ConA monomer. A *purple* ribbon model of ConA (molecule A) is shown. The bound Mn^{2+} (S1) and Ca^{2+} (S2) are shown as *large gray* and *black spheres*, respectively. *B*, comparison between VIP36 and ConA metal-binding site structures. The VIP36 (molecule A) and ConA structures are colored *yellow* and *purple*, respectively. Residues of VIP36 and ConA are labeled in *black* and *purple*, respectively. The Ca^{2+} in VIP36 is shown as a *large pink sphere*. Because the position of Ca^{2+} at the S2 site in ConA is almost the same as in VIP36, it is not shown. Water molecules found in the S1 site of ConA are shown as *small white spheres* and are labeled *W3* and *W4*. *C*, overall structure of ERGIC-53 CRD. A *cyan* ribbon model of ERGIC-53 (molecule A) is shown. The bound Ca^{2+} is shown as *large magenta spheres* (M1 and M2). *D*, comparison between VIP36 (*yellow*) and ERGIC-53 (*cyan*) Ca^{2+}-binding site structures. Because the position of Ca^{2+} at the M2 site in ERGIC-53 is almost the same as in VIP36, it is not shown. Water molecules found in the M1 site of ERGIC-53 are shown as *small orange spheres* and are labeled *W5* and *W6*. Residues involved in the metal binding are shown as *ball-and-stick* models.

no disulfide-linked or stable non-covalent oligomers of recombinant exoplasmic/luminal domain (residues 45–322) or endogenous VIP36 could be detected by cross-linking or sedimentation analysis (46). Furthermore we confirmed that the exoplasmic/luminal domain of VIP36 (residues 51–301 and 51–322) is monomeric in physiological solution by gel filtration analyses (supplemental Fig. 1). Indeed the stalk domain (residues 279–322) of VIP36 is 95–162 residues shorter than those of ERGIC-53, Emp46p, and Emp47p. The portion of the stalk domain of VIP36 included in our construct (residues 279–301) does not form coiled-coil structure (Fig. 2*A* and supplemental Fig. 2). The short stalk domain and the absence of coiled-coil domain suggest that VIP36 may likely function as a monomer.

It is known that leguminous lectins coordinate Mn^{2+} and Ca^{2+} ions, termed S1 and S2, respectively, in their β-sandwich structures (Fig. 6, *A* and *B*) (47). The S1 ion stabilizes the S2-binding site, and the S2 ion fixes the positions of the amino acids that interact with the oligosaccharide ligands. In this study, we showed that VIP36 has a single Ca^{2+} in the CRD structures and that the Ca^{2+} fixes the positions of Asp^{131}, Asn^{166}, and His^{190} that interact with carbohydrate ligands in the primary binding site (Figs. 3 and 5). Specifically significant conformational changes upon Ca^{2+} binding take place around the Ca^{2+} and primary carbohydrate-binding site of VIP36 (Fig. 3). Similar but more pronounced structural changes of the corresponding site upon metal binding were also observed in concanavalin A (ConA) (48) and ERGIC-53 (23). The Ca^{2+} of ConA induces large conformational changes to stabilize the correct geometry of the Ca^{2+}-binding site that comprise the *trans* to *cis* isomerization of the Ala^{207}-Asp^{208} peptide bond accompanied by the formation of the carbohydrate-binding site (48). In VIP36 structures, such isomerization changes were not observed. We also observed that Ca^{2+} is required for interaction between VIP36 and $Man_6(GlcNAc)_2$-Asn by SPR experiments (supplemental Fig. 3). These results explain the Ca^{2+}-dependent carbohydrate binding of VIP36.

It was shown that ERGIC-53 contains two Ca^{2+} ions termed M1 and M2 (Fig. 6, *C* and *D*) and that the M1 ion does not lie at the same site as the S1 ion, although M2 is located at the corresponding S2 site (23). The Ca^{2+} of VIP36 corresponds to the M2 site of ERGIC-53. When the VIP36 and ERGIC-53 structures are superimposed, the M2 metal ions overlay with a separation that is less than 0.2 Å. Although the Ca^{2+} of VIP36 is equivalent to the M2 site of ERGIC-53, the electron density maps of VIP36 show no peak that could be assigned as a metal ion either at the corresponding M1 site or at any other sites within the structure. In the Ca^{2+}-binding site (M2 and S2), the Ca^{2+}-coordinating residues are structurally very well conserved except for Asp^{193} in VIP36 (Fig. 6, *B* and *D*). The corresponding Asp^{19} (ConA) and Asp^{189} (ERGIC-53) residues are coordinated by the two metal ions. In VIP36, the Oδ-1 of Asp^{193} forms a hydrogen bond with the main-chain nitrogen atom of Asp^{167} to stabilize the Ca^{2+}-binding site. As a result, only one Ca^{2+} ion fixes the ligand binding residues in VIP36. Our crystallographic studies also suggest that VIP36 did not bind other divalent cations, neither Mn^{2+} nor Mg^{2+} (data not shown). Loop 1 of VIP36 is two residues longer than that of ERGIC-53. Likewise the residues coordinating the M1 ion in ERGIC-53 (Asp^{163}, Asp^{165},

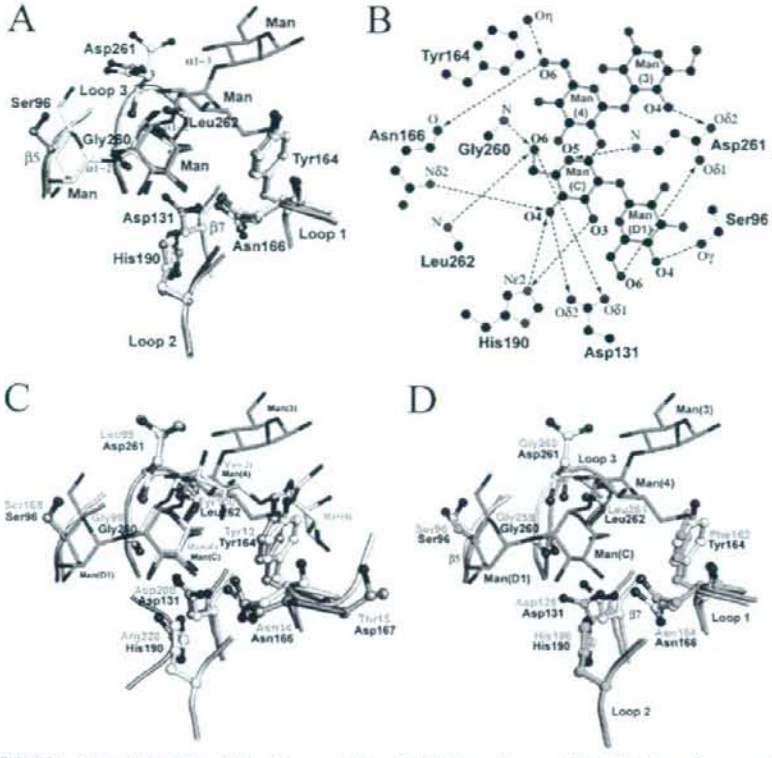

FIGURE 7. *A*, superimposition of Man-, Man_2-, and $Man_3GlcNAc$-bound forms of VIP36. The Man-, Man_2-, and $Man_3GlcNAc$-bound forms of VIP36 (molecule A) are colored in *marine blue*, *white*, and *yellow*, respectively. The bound Man, Man_2, and Man_3 are shown as *magenta*, *white*, and *green stick* models, respectively. *B*, ligand binding diagram. The model of Man-α-1,2-Man-α-1,2-Man-α-1,3-Man (Man_4) is designated as Man(D1)-Man(C)-Man(4)-Man(3), respectively. Hydrogen bonds are indicated with *dotted arrows* pointing in the direction from donor to acceptor. *C*, comparison between the VIP36 (*yellow*) and ConA (*purple*) carbohydrate ligand-binding site. Residues binding to the ligands are shown in *ball-and-stick* models. *D*, comparison between the VIP36 (*yellow*) and ERGIC-53 (*cyan*) carbohydrate ligand-binding site. The model of Man_4 is shown as a *green stick* model. Residues of VIP36 binding to the ligands and the corresponding ones in ERGIC-53 are shown in *ball-and-stick* models.

Asn^{169}, Asn^{170}, and Asp^{189}; shown in green in supplemental Fig. 2) are poorly conserved in VIP36. Taken together, we conclude that VIP36 binds only one Ca^{2+} ion and that the single Ca^{2+} fixes the positions of residues involved in carbohydrate ligand binding.

Our crystallographic studies reveal extensive interactions between VIP36 and Man-α-1,2-Man-α-1,2-Man residues of the D1 arm of high mannose type glycans. Based on the Man-, Man_2-, and $Man_3GlcNAc$-bound structures, a model structure of VIP36 in complex with Man-α-1,2-Man-α-1,2-Man-α-1,3-Man (Man_4) was built and then designated as Man(D1)-Man(C)-Man(4)-Man(3), respectively (Fig. 7). The carbohydrate-binding site is located in a negatively charged pocket (Fig. 2*B*). The extended carbohydrate-binding site comprises β5, β7, and Loops 1, 2, and 3. The mannose residue in the primary binding site corresponds to the Man(C) moiety at the middle of the D1 arm. In addition, Asp^{261} is flexible in mannose recognition and can flip between Man(3) and Man(D1) depending on the local environment (supplemental Fig. 4). The crystallographic results correlate well with the SPR experiments (Fig. 4) and the previous results (19, 20) that VIP36 recognizes Man-α-1,2-Man-α-1,2-Man residues of the D1 arm of high mannose type glycans.

Next the carbohydrate-binding site of VIP36 was compared with that of ConA in complex with Man-α-1,3-(Man-α-1,6-)Man (corresponding to Man(3)-(Man(4'))-Man(4)) (49). Although the carbohydrate binding specificity of VIP36 and ConA is essentially different, the structural conservation of ligand-binding sites between them is observed in not only the Man(C)-binding site but also the Man(D1)- and Man(4)-binding sites of VIP36 (Fig. 7*C*). In the Man(C)-binding site of VIP36, the ligand binding residues are structurally very well conserved except for His^{190} in VIP36 (Fig. 7*C*). The corresponding main-chain nitrogen atom of Arg^{228} in ConA is bound to only the 3-OH group of the mannose residue. In contrast, Nε-2 of His^{190} in VIP36 is bound to the 3-OH and 4-OH groups and acts simultaneously as hydrogen bond donor and acceptor (Fig. 7*B*). In the Man(4)-binding site, although the carbohydrate binding loop conformation of VIP36 is largely different than that of ConA, the side-chain position of Tyr^{164} is very similar to that of Tyr^{12} in ConA.

When the carbohydrate-binding site of VIP36 was compared with the corresponding site of ERGIC-53 in complex with Ca^{2+} (23), the Man_4 binding residues of VIP36 are largely identical to the corresponding residues of ERGIC-53 (Fig. 7*D* and supplemental Fig. 2). The structural conservation suggests that ERGIC-53 also binds the D1 arm moiety of high mannose type glycoproteins, which is consistent with the function of ERGIC-53 as a transport lectin for high mannose type glycoproteins. These contain $Man_8(GlcNAc)_2$ with an intact D1 arm and are transported from the ER by the ER quality control mechanism (2, 3). However, there are some structural differences in the β5, β7, and Loops 1 and 3 regions: (i) in β5 the side-chain orientation of Ser^{96} of ERGIC-53 is dissimilar to that of VIP36, (ii) the side-chain orientation of Asp^{129} in β7 of ERGIC-53 is different than that of the corresponding Asp^{131} of VIP36, (iii) Phe^{162} of ERGIC-53 is replaced by Tyr^{164} in VIP36, and (iv) the Loop 3 of ERGIC-53 is positioned further away from the ligand when compared with VIP36, and Asp^{261} of VIP36 is replaced by Gly^{260} in ERGIC-53. Most significantly, Tyr^{164} and Asp^{261} in VIP36 are better suited than Phe^{162} and Gly^{260} in ERGIC-53 for binding to the Man_4. In ERGIC-53, the

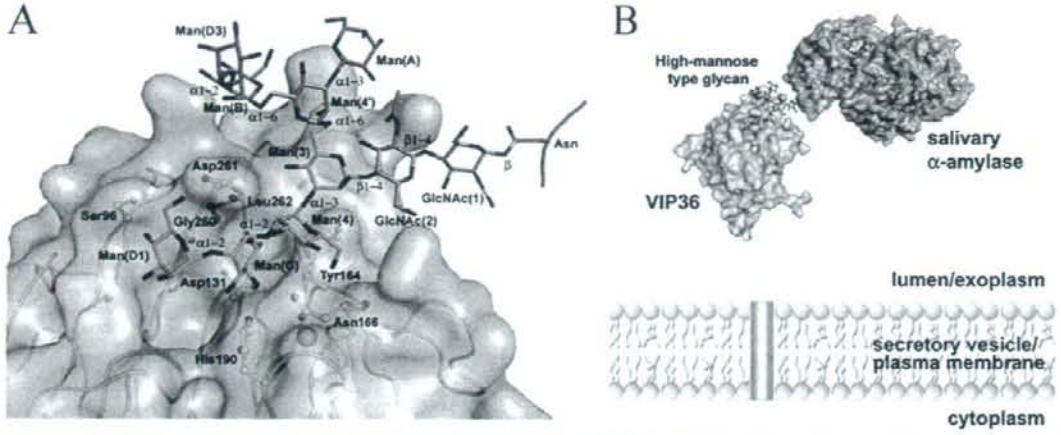

FIGURE 8. **Model for binding between VIP36 and high mannose type glycan ($Man_8(GlcNAc)_2$-Asn).** *A*, the high mannose type glycan is indicated by a *stick* model. In the oligosaccharide, the part determined in this study is colored in *green*. The modeled D2 and D3 arms and *N*-linked chitobiose moiety of the high mannose type glycan are shown in *purple*. The types of glycosidic linkages are also indicated. The individual carbohydrate residues of $Man_8(GlcNAc)_2$-Asn are shown as in Fig. 1. Residues involved in the ligand binding are shown as *ball-and-stick* models. *B*, model for binding between VIP36 and salivary α-amylase carrying $Man_8(GlcNAc)_2$ in rat secretory vesicles.

presumptive weak interactions between ERGIC-53 and carbohydrate ligands might be compensated by the oligomerization of the CRDs.

To demonstrate that the crystal structure strictly represents the complex formed in solution, we simulated a complex model of $Man_8(GlcNAc)_2$-Asn and VIP36 (Fig. 8*A*). In this model, there are no significant steric clashes between high mannose type *N*-glycan and VIP36. The monomeric VIP36 seems to accommodate the glycan along an extended ligand-binding site. Kamiya *et al.* (20) have suggested that VIP36 recognizes the D1 arm and showed that mannose trimming and monoglucosylation of the D1 arm resulted in significant reduction in affinity for VIP36 CRD using frontal affinity chromatography analysis. When a glucose residue is modeled into the VIP36·Man_4 structure at the Man(D1) position through α1–3 linkage, a steric hindrance occurs between the glucose and Glu^{98} of VIP36 (data not shown). In addition, we have shown that VIP36 recognizes the D1 arm, Man-α-1,2-Man-α-1,2-Man, using SPR analysis (Fig. 4) and that Asp^{131} of VIP36 plays an essential role in binding ^{35}S-labeled secretory glycoproteins (13). Kawasaki *et al.* (21) have also shown that Asp^{131} of VIP36 was involved in ligand binding using a flow cytometry-based method. On the other hand, it was shown that Asp^{121}, Asn^{156}, and His^{178} of human ERGIC-53, which correspond to Asp^{131}, Asn^{166}, and His^{190} of VIP36, are involved with binding to mannose and its cargo glycoprotein, cathepsin Z-related protein (15, 18, 50). From these observations, we conclude that the interaction between VIP36 and high mannose type glycans in solution is also achieved through interactions between these amino acid residues and the D1 arm.

It has been shown that VIP36 recycles between the ER and the Golgi complex (9–11). To date, however, there is no obvious evidence that VIP36 is involved in retrograde transport of glycoproteins from the Golgi complex to the ER. On the other hand, we revealed that VIP36 localizes in the *trans*-Golgi network (12) and is involved in secretion of high mannose type glycoproteins clusterin and α-amylase (13, 14). It has been generally known that the D1 arm is trimmed by *cis*-Golgi mannosidase I to form $Man_5(GlcNAc)_2$ in the *cis*-Golgi. The carbohydrate structure has a lower affinity for VIP36 (19, 20). In this study, we have shown that VIP36 specifically binds the Man-α-1,2-Man-α-1,2-Man residues of the D1 arm of high mannose type glycan. Taken together, VIP36 might be involved in anterograde transport of certain glycoproteins carrying high mannose type glycan with the D1 arm from the ERGIC via the Golgi complex to the plasma membrane by protecting the D1 arm against trimming by *cis*-Golgi mannosidase I. Although it is not known whether or not high mannose type glycan of rat salivary α-amylase has the D1 arm, a possible model for binding between VIP36 and salivary α-amylase carrying high mannose type glycan ($Man_8(GlcNAc)_2$) in rat parotid acinar cells is shown (Fig. 8*B*).

In summary, we determined the first complex structure of the exoplasmic/luminal domain of the transport lectin VIP36 and Ca^{2+} and Man, Man_2, and $Man_3GlcNAc$, which are part of the D1 arm of high mannose type glycans. Our results provide structural insights into the mechanism of recognition of high mannose type glycoproteins by VIP36 in a Ca^{2+}-dependent and D1 arm-specific manner. Further biochemical analysis such as subcellular localization of VIP36 on a wide variety of cells and identification of its cargo glycoproteins together with the detailed carbohydrate structures will provide further insight into the mechanism of high mannose type glycoprotein transport by VIP36.

Acknowledgments—We thank Drs. L. M. G. Chavas and K. Ihara for helpful discussion and the beamline staff of BL-5A, BL-6A, and AR-NW12A at the Photon Factory, High Energy Accelerator Research Organization (KEK), Tsukuba, Japan (Proposals 2003S2002, 2005G070, and 2006S2006) for providing the data collection facilities and support.

REFERENCES

1. Fiedler, K., and Simons, K. (1995) *Cell* **81,** 309–312
2. Helenius, A., and Aebi, M. (2001) *Science* **291,** 2364–2369
3. Schrag, J. D., Procopio, D. O., Cygler, M., Thomas, D. Y., and Bergeron, J. J. (2003) *Trends Biochem. Sci.* **28,** 49–57
4. Ghosh, P., Dahms, N. M., and Korfeld, S. (2003) *Nat. Rev. Mol. Cell Biol.* **4,** 202–212
5. Hauri, H. P., Kappeler, F., Andersson, H., and Appenzeller, C. (2000) *J. Cell Sci.* **113,** 587–596
6. Zhang, B., Cunningham, M. A., Nichols, W. C., Bernat, J. A., Seligsohn, U., and Pipe, S. W. (2003) *Nat. Genet.* **34,** 22022–22025
7. Sato, K., and Nakano, A. (2002) *Mol. Biol. Cell* **13,** 2518–2532
8. Fiedler, K., White, J., Grill, S., Füllekrug, J., and Stelzer, E. H. (1994) *EMBO J.* **13,** 1729–1740
9. Füllekrug, J., Scheiffele, P., and Simons, K. (1999) *J. Cell Sci.* **112,** 2813–2821
10. Dahm, T., White, J., Grill, S., Füllekrug, J., and Stelzer, E. H. (2001) *Mol. Biol. Cell* **12,** 1481–1498
11. Shimada, O., Hara-Kuge, S., Yamashita, K., Tosaka-Shimada, H., Yanchao, L., Yongnan, L., Atsumi, S., and Ishikawa, H. (2003) *Cell Struct. Funct.* **28,** 155–163
12. Shimada, O., Hara-Kuge, S., Yamashita, K., Tosaka-Shimada, H., Yanchao, L., Einan, L., Atsumi, S., and Ishikawa, H. (2003) *J. Histochem. Cytochem.* **51,** 1057–1063
13. Hara-Kuge, S., Ohkura, T., Ideo, H., Shimada, O., Atsumi, S., and Yamashita, K. (2002) *J. Biol. Chem.* **277,** 16332–16339
14. Hara-Kuge, S., Seko, A., Shimada, O., Tosaka-Shimada, H., and Yamashita, K. (2004) *Glycobiology* **14,** 739–744
15. Appenzeller, C., Andersson, H., Kappeler, F., and Hauri, H. P. (1999) *Nat. Cell Biol.* **1,** 330–334
16. Moussalli, M., Pipe, S. W., Hauri, H. P., Nichols, W. C., Ginsburg, D., and Kaufman, R. J. (1999) *J. Biol. Chem.* **274,** 32539–32542
17. Appenzeller-Herzog, C., Nyfeler, B., Burkhard, P., Santamaria, I., Lopez-Otin, C., and Hauri, H. P. (2005) *Mol. Biol. Cell* **16,** 1258–1267
18. Appenzeller-Herzog, C., Roche, A. C., Nufer, O., and Hauri, H. P. (2004) *J. Biol. Chem.* **279,** 12943–12950
19. Hara-Kuge, S., Ohkura, T., Seko, A., and Yamashita, K. (1999) *Glycobiology* **9,** 833–839
20. Kamiya, Y., Yamaguchi, Y., Takahashi, N., Arata, Y., Kasai, K. I., Ihara, Y., Matsuo, I., Ito, Y., Yamamoto, K., and Kato, K. (2005) *J. Biol. Chem.* **280,** 37178–37182
21. Kawasaki, N., Matsuo, I., Totani, K., Nawa, D., Suzuki, N., Yamaguchi, D., Matsumoto, N., Ito, Y., and Yamamoto, K. (2007) *J. Biochem. (Tokyo)* **141,** 221–229
22. Velloso, L. M., Svensson, K., Schneider, G., Pettersson, R. F., and Lindqvist, Y. (2002) *J. Biol. Chem.* **277,** 15979–15984
23. Velloso, L. M., Svensson, K., Pettersson, R. F., and Lindqvist, Y. (2003) *J. Mol. Biol.* **334,** 845–851
24. Satoh, T., Sato, K., Kanoh, A., Yamashita, K., Yamada, Y., Igarashi, N., Kato, R., Nakano, A., and Wakatsuki, S. (2006) *J. Biol. Chem.* **281,** 10410–10419
25. Beignet, J., Tiernan, J., Woo, C. H., Kariuki, B. M., and Cox, L. R. (2004) *J. Org. Chem.* **69,** 6341–6356
26. Peters, T. (1991) *Liebigs Ann. Chem.* 135–141
27. Dromer, F., Chevalier, R., Sendid, B., Improvisi, L., Jouault, T., Robert, R., Mallet, J. M., and Poulain, D. (2002) *Antimicrob. Agents Chemother.* **46,** 3869–3876
28. Meuwly, R., and Vasella, A. (1986) *Helv. Chim. Acta* **69,** 25–34
29. Allerhand, A., and Berman, E. (1984) *J. Am. Chem. Soc.* **106,** 2412–2420
30. Tanimoto, T., Ikuta, A., Sugiyama, M., and Koizumi, K. (2002) *Chem. Pharm. Bull. (Tokyo)* **50,** 280–283
31. Yamashita, K., Tachibana, Y., Mihara, K., Okada, S., Yabuuchi, H., and Kobata, A. (1980) *J. Biol. Chem.* **255,** 5126–5133
32. Tai, T., Yamashita, K., Ogata-Arakawa, M., Koide, N., Muramatsu, T., Iwashita, S., Inoue, Y., and Kobata, A. (1975) *J. Biol. Chem.* **250,** 8569–8575
33. Hiraki, M., Kato, R., Nagai, M., Satoh, T., Hirano, S., Ihara, K., Kudo, N., Nagae, M., Kobayashi, M., Inoue, M., Uejima, T., Oda, S., Chavas, L. M., Akutsu, M., Yamada, Y., Kawasaki, M., Matsugaki, N., Igarashi, N., Suzuki, M., and Wakatsuki, S. (2006) *Acta Crystallogr. Sect. D Biol. Crystallogr.* **62,** 1058–1065
34. Otwinowski, Z., and Minor, W. (1997) *Methods Enzymol.* **276,** 307–326
35. Vagin, A., and Teplyakov, A. (1997) *J. Appl. Crystallogr.* **30,** 1022–1025
36. Brünger, A. T., Adams, P. D., Clore, G. M., DeLano, W. L., Gros, P., Grosse-Kunstleve, R. W., Jiang, J. S., Kuszewski, J., Nilges, M., Pannu, N. S., Read, R. J., Rice, L. M., Simonson, T., and Warren, G. L. (1998) *Acta Crystallogr. Sect. D Biol. Crystallogr.* **54,** 905–921
37. Murshudov, G. N. (1997) *Acta Crystallogr. Sect. D Biol. Crystallogr.* **53,** 240–255
38. Emsley, P., and Cowtan, K. (2004) *Acta Crystallogr. Sect. D Biol. Crystallogr.* **60,** 2126–2132
39. Laskowski, R. A., MacArthur, M. W., Moss, D. S., and Thornton, J. M. (1993) *J. Appl. Crystallogr.* **26,** 283–291
40. Nicholls, A., Sharp, K. A., and Honig, B. (1991) *Proteins Struct. Funct. Genet.* **11,** 281–296
41. Wallace, A. C., Laskowski, R. A., and Thornton, J. M. (1995) *Protein Eng.* **8,** 127–134
42. DeLano, W. (2002) *The PyMOL Molecular Graphics System*, DeLano Scientific, San Carlos, CA
43. Weis, W. I., and Drickamer, K. (1996) *Annu. Rev. Biochem.* **65,** 441–473
44. Neve, E. P. A., Lahtinen, U., and Pettersson, R. F. (2005) *J. Mol. Biol.* **354,** 556–568
45. Sato, K., and Nakano, A. (2003) *Mol. Biol. Cell* **14,** 3055–3063
46. Fiedler, K., and Simons, K. (1995) *J. Cell Sci.* **109,** 271–276
47. Rini, J. M., Hardman, K. D., Einspahr, H., Suddath, F. L., and Carver, J. P. (1993) *J. Biol. Chem.* **268,** 10126–10132
48. Bouckaert, J., Poortmans, F., Wyns, L., and Loris, R. (1996) *J. Biol. Chem.* **271,** 16144–16150
49. Naismith, J. H., and Field, R. A. (1996) *J. Biol. Chem.* **271,** 972–976
50. Itin, C., Roche, A. C., Monsigny, M., and Hauri, H. P. (1996) *Mol. Biol. Cell* **7,** 483–493

Plant Cell Physiol. 48(7): 948–957 (2007)
doi:10.1093/pcp/pcm064, available online at www.pcp.oxfordjournals.org

Expression of the Algal Cytochrome c_6 Gene in *Arabidopsis* Enhances Photosynthesis and Growth

Hirotaka Chida [1], Aiko Nakazawa [1], Hideharu Akazaki [1], Takako Hirano [1], Kohei Suruga [1], Masahiro Ogawa [1], Tadashi Satoh [1], Kazunari Kadokura [1], Seiji Yamada [1], Wataru Hakamata [1], Katsunori Isobe [2], Tei-ichiro Ito [1], Ryuichi Ishii [2], Toshiyuki Nishio [1], Kintake Sonoike [3] and Tadatake Oku [1,*]

[1] *Bio-organic Chemistry Laboratory, Graduate School of Bioresource Sciences, Nihon University, Kameino 1866, Fujisawa-shi, Kanagawa, 252-8510 Japan*
[2] *Laboratory of Crop Science, Graduate School of Bioresource Sciences, Nihon University, Kameino 1866, Fujisawa-shi, Kanagawa, 252-8510 Japan*
[3] *Department of Integrated Biosciences, Graduate School of Frontier Sciences, University of Tokyo, Box 101, 5-1-5 Kashiwanoha, Kashiwa-shi, Chiba, 277-8562 Japan*

Photosynthetic plants convert light energy into ATP and NADPH in photosynthetic electron transfer and photophosphorylation, and synthesize mainly carbohydrates in the Calvin–Benson cycle. Here we report the enhancement of photosynthesis and growth of plants by introducing the gene of an algal cytochrome c_6, which has been evolutionarily eliminated from higher plant chloroplasts, into the model plant *Arabidopsis thaliana*. At 60 d after planting, the plant height, leaf length and root length of the transformants were 1.3-, 1.1- and 1.3-fold those in the wild-type plants, respectively. At the same time, in the transgenic plants, the amounts of chlorophyll, protein, ATP, NADPH and starch were 1.2-, 1.1-, 1.9-, 1.4- and 1.2-fold those in the wild-type plants, respectively. The CO_2 assimilation capacity of the transgenic plants was 1.3-fold that of the wild type. Moreover, in transgenic *Arabidopsis* expressing algal cytochrome c_6, the $1-qP$, which reflects the reduced state of the plastoquinone pool, is 30% decreased compared with the wild type. These results show that the electron transfer of photosynthesis of *Arabidopsis* would be accelerated by the expression of algal cytochrome c_6. Our results demonstrate that the growth and photosynthesis of *Arabidopsis* plants could be enhanced by the expression of the algal cytochrome c_6 gene.

Keywords: *Arabidopsis thaliana* — Cytochrome c_6 — Electron transport — Photosynthesis — Transgenic plant.

Abbreviations: Cyt, cytochrome; PAM, pulse amplitude-modulated; PC, plastocyanin; RT–PCR, reverse transcription–PCR; TAIL-PCR, thermal asymmetric interlaced PCR.

Introduction

The hemeprotein cytochrome (Cyt) c_6 and/or copper protein plastocyanin (PC) transfer electrons between the Cyt b_6f complex and the PSI reaction center complex in the algal photosynthetic electron transport chain (Katoh 1960a, Katoh and Takamiya 1961). Although the structures of the two proteins are totally different, they are approximately the same in terms of molecular weight and redox potential (Ullmann et al. 1997, Kerfeld and Krogman 1998). Cyt c_6 (formerly named Cyt c_{553}) was first prepared and crystallized from a red alga in 1960 (Katoh 1960b). In some cyanobacteria and green algae, Cyt c_6 replaces PC in response to copper deficiency (Merchant and Bogorad 1987). On the other hand, this does not occur in land plants, and it is widely accepted that Cyt c_6 has been evolutionarily eliminated from land plants (Sigfridsson 1998, De la Rosa et al. 2002). However, in 2002, genomic analysis and expressed sequence tag (EST) analysis revealed a gene encoding Cyt c_6-like protein (Cyt c_{6A} or Cyt c_P) in higher plants (Wastl et al. 2002, De la Rosa et al. 2006, Howe et al. 2006). Although it was proposed that Cyt c_{6A} could substitute for PC in electron transfer in *Arabidopsis* (Gupta 2002), electron transfer experiments and a genetic analysis of *Arabidopsis* mutants (Molina-Heredia et al. 2003, Weigel et al. 2003) directly opposed this view. On the basis of the tertiary structure of Cyt c_{6A} and on its low redox potential, we also showed that the Cyt c_{6A} is an unsuitable electron donor between Cyt b_6f and PSI (Chida et al. 2006). We assume that PC is the only electron carrier that is effectively working in vivo.

There are many reports on introducing genes of Calvin–Benson cycle enzymes of photosynthesis into plants, but there are only a few studies, which have shown an enhancement of carbon dioxide (CO_2) fixation and growth in transgenic plants (Ku et al. 1999, Miyagawa et al. 2001). On the other hand, in the photosynthetic electron transfer and photophosphorylation of plants, there have been very few reports on the enhancement of photosynthesis and growth based on the increase in NADPH by gene induction (Rodriguez et al. 2007), but no reports on that of ATP.

*Corresponding author: E-mail, oku@brs.nihon-u.ac.jp; Fax, +81-466-84-3950.

Here, we try to introduce the algal Cyt c_6 gene into the model plant *Arabidopsis thaliana*, thus going back in the evolutionary history of plants. Electron transfer of red algal Cyt c_6 and *Arabidopsis* PC to *Arabidopsis* PSI is first examined in vitro, and we subsequently introduce the *Porphyra yezoensis* Cyt c_6 gene into the higher plant *A. thaliana*. We demonstrate that the expression of Cyt c_6 in addition to that of PC in chloroplasts leads to a high growth rate measured in terms of height, root and leaf lengths, an increase in the amounts of chlorophyll, proteins, ATP, NADPH and starch, and an increase in the capacity for CO_2 assimilation and the efficiency of photosynthetic electron transfer. We report here the reinforcement of photosynthetic electron transfer and photophosphorylation by introducing the algal Cyt c_6 gene into *A. thaliana*.

Results

Electron transfer of Porphyra Cyt c_6 to Arabidopsis PSI in vitro

Cyt c_6 from the red alga *P. yezoensis* was selected for in vitro experiments, since the midpoint redox potential of this cytochrome (+371 mV) (Yamada et al. 2000, Satoh et al. 2002) is similar to that of *A. thaliana* PC (+381 mV) (Molina-Heredia et al. 2003). Photooxidation of P700, the reaction center chlorophyll of PSI, can be monitored by the increase in the absorbance at 820 nm upon illumination by a xenon flash. P700 could be re-reduced by Cyt c_6 or PC, which is the soluble electron donor for PSI, in a concentration-dependent manner (Hervás et al. 1994). To investigate whether algal Cyt c_6 could substitute for the land plant PC in its physiological role, we performed a flash-induced kinetic analysis of the *A. thaliana* PSI preparation with *P. yezoensis* Cyt c_6 and *A. thaliana* PC. The half decay times of dark relaxation of the absorbance change due to P700 in the presence of 10 μM *P. yezoensis* Cyt c_6 were 4.4-fold shorter than those of *A. thaliana* PC (Fig. 1). The differences between the half decay times were 3.1-, 3.0-, 3.9-, 3.9- and 4.4-fold at concentrations of electron donors of 1, 2, 5, 15 and 20 μM, respectively. These results indicate that the *Porphyra* Cyt c_6 can effectively transfer an electron to *Arabidopsis* PSI.

Development of transgenic Arabidopsis having Porphyra Cyt c_6

We produced transgenic *Arabidopsis* plants expressing the *Porphyra* Cyt c_6 gene, which reduces *Arabidopsis* PSI more efficiently compared with *Arabidopsis* PC in in vitro experiments as described above. To target Cyt c_6 into the chloroplast lumen, we constructed a plasmid containing the Cyt c_6 gene from the red alga *P. yezoensis* with the *petE* (plastocyanin) transit peptides (Hageman et al. 1986, Soll and Schleiff 2004) from *A. thaliana* (Fig. 2a). The constructed plasmid DNA was introduced into the *A. thaliana* plants by the *Agrobacterium* method (Dandekar and Fisk 2005). Genomic DNA from several transformed plants was isolated and analyzed by PCR to check if the Cyt c_6 gene was inserted into the genome (Fig. 2b). Approximately 0.5% of the analyzed primary transgenic plants (T_1) had the insertion. Total RNA and poly(A)$^+$ mRNA were isolated from leaves of Cyt c_6 gene-positive T_1 transformant and wild-type *Arabidopsis* plants. Two oligonucleotide primers, AtPcsig1 and Pyc62 (see Materials and Methods), were used in a reverse transcriptase–PCR (RT–PCR) to amplify and detect the mRNA transcript of the Cyt c_6 gene. The transgenic plants that harbored the Cyt c_6 gene exhibited a full-length Cyt c_6 mRNA transcript that corresponds to a theoretical length of 490 bp (Fig. 2c). The expression of Cyt c_6 in the chloroplast of *Arabidopsis* could be detected by Western blot analysis of chloroplast protein extracts. Cyt c_6 purified from *P. yezoensis* was used as a positive control. A 9.6 kDa protein that cross-reacted with Cyt c_6 antiserum was present in T_1 transgenic *A. thaliana* or *P. yezoensis*, but was absent

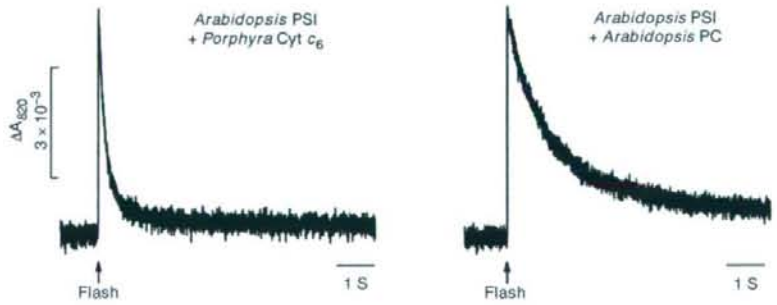

Fig. 1 Kinetic trace of *Arabidopsis* PSI reduction by *Porphyra* Cyt c_6 and *Arabidopsis* plastocyanin in vitro. The PSI particles were isolated from *A. thaliana*. The metalloprotein concentration was 10 μM. Other conditions were as described under Materials and Methods.

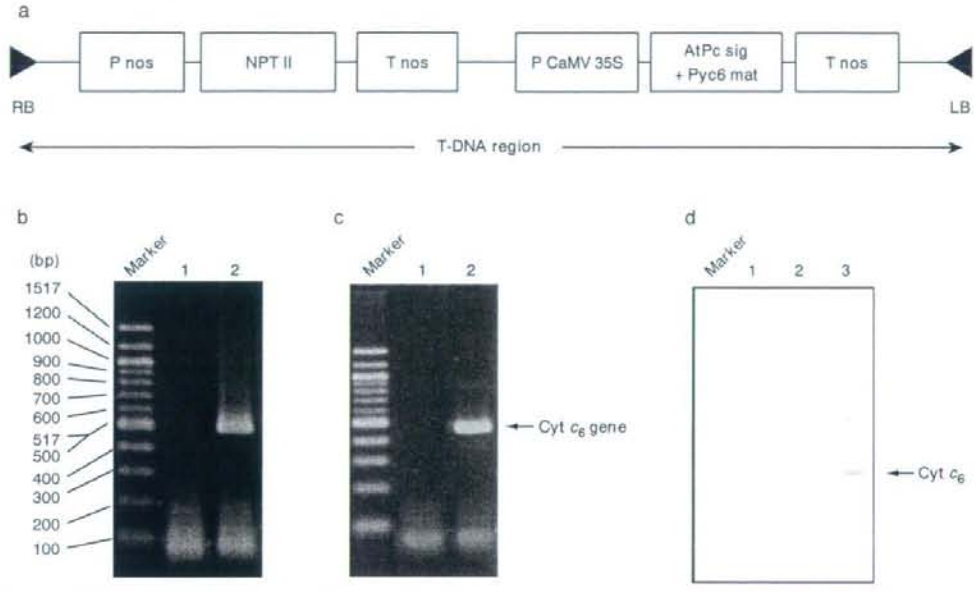

Fig. 2 Construction of *Porphyra* Cyt c_6-transformed *Arabidopsis*. (a) Construct of plasmid DNA. P nos, nopaline synthase promoter; NPT II, neomycin phosphotransferase; T nos, nopaline synthase terminator; P CaMV 35S, cauliflower mosaic virus 35S promoter; AtPc sig, *A. thaliana* plastocyanin transit peptides; Pyc6 mat, *P. yezoensis* cytochrome c_6 mature peptides; LB, left T-DNA border; RB, right T-DNA border. (b) Amplification of the Cyt c_6 gene in wild-type (1) and transgenic (2) plants using PCR. (c) RT–PCR analysis of wild-type (1) and transgenic (2) plants. (d) Western blot analysis of chloroplast proteins of wild-type (1) and transgenic (2) plants, and *P. yezoensis* (3).

in the wild-type control (Fig. 2d). In the chloroplasts of transgenic *Arabidopsis*, the level of Cyt c_6 corresponds to 1.2-fold that of PC when compared in terms of the molar ratio (Kieselbach et al. 1998, Navarro et al. 2004). The secondary transgenic plants (T_2) that were harvested from the T_1 transformants were used for further analysis. Approximately 90% of seeds harvested from the T_1 transformants were Cyt c_6 gene-positive, and the T_2 transformants gave the same experimental results as the T_1 transformants. The integration of T-DNA was detected by thermal asymmetric interlaced (TAIL)-PCR (Liu et al. 1995, Liu et al. 2005), which revealed its location at approximately 13.7 Mbp from the top of chromosome 3 in *A. thaliana* of mutant line A. There are no intrinsic genes.

Expression of Porphyra Cyt c_6 is effective for enhancing growth of Arabidopsis

To examine the change in the growth of transgenic plants expressing the *Porphyra* Cyt c_6 gene, we measured plant height, leaf and root lengths and the number of flowers using 20 wild-type and transgenic plants. The changes in growth were measured every 10 d from 10 to 90 d after cultivation. The height of the transgenic plants (T_2) expressing Cyt c_6 was significantly greater than that of the wild-type plants from 30 to 80 d after planting (t-test, $P<0.05$) (Fig. 3a). In particular, at 40 and 60 d after planting, the transgenic plants showed 1.9- and 1.3-fold increases in height, respectively, compared with the wild-type plants (Fig. 3a, c, e). The hypocotyl elongation of the transgenic plants also started 7–10 d earlier than that of the wild-type plants. As shown in Fig. 3b, d and f, increased leaf length was also observed in the transgenic plants. The leaf length of the transgenic plants was significantly larger than that of the wild type from 40 to 70 d after planting (t-test, $P<0.05$). The final levels of both the plant height and leaf length were the same between the wild types and the transgenic plants. The root lengths of the transgenic *Arabidopsis* plants grown hydroponically were significantly larger than those of the wild-type plants from 30 to 70 d after planting (t-test, $P<0.05$) (Fig. 4a). The 1.4- and 1.3-fold increase in the root lengths was observed on 40 and 60 d after planting, respectively (Fig. 4a, b, c). The final root length at 80 and 90 d after planting was not different between the transgenic plants and the wild-type plants.

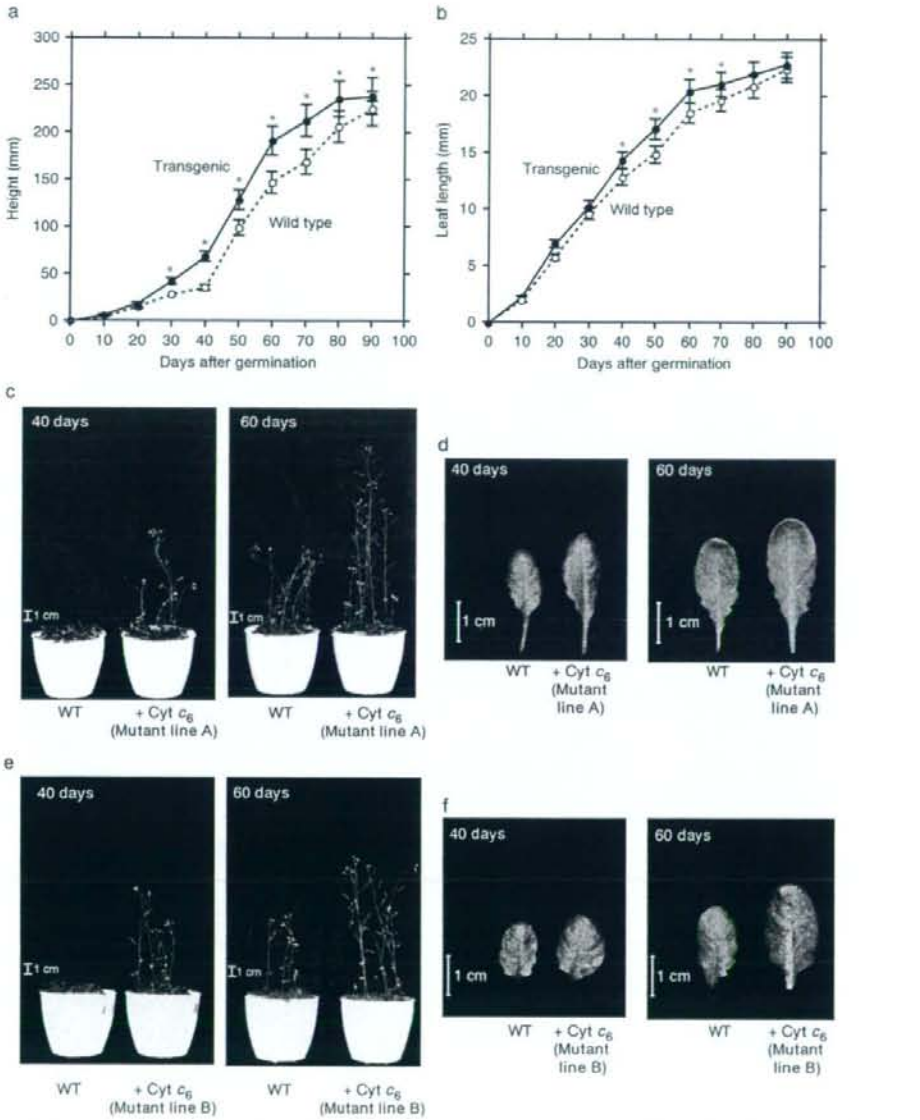

Fig. 3 Plant growth. (a) Time courses of the plant height of wild-type (open circles) and transgenic (filled circles) plants (mutant line A) in 360 p.p.m. CO_2 at 50 μmol photons $m^{-2} s^{-1}$. (b) Time courses of leaf lengths of wild-type (open circles) and transgenic (filled circles) plants (mutant line A). (c) Wild-type and transgenic *Arabidopsis* plants of mutant line A were photographed after 40 and 60 d. (d) The leaf lengths of wild-type and transgenic *Arabidopsis* plants of mutant line A were photographed after 40 and 60 d. (e) Wild-type and transgenic *Arabidopsis* plants of mutant line B were photographed after 40 and 60 d. (f) The leaf lengths of wild-type and transgenic *Arabidopsis* plants of mutant line B were photographed after 40 and 60 d. The bars correspond to the SD from 20 plants in each experiment. Asterisks indicate that the difference between wild-type and transgenic plants was significant by a *t*-test ($P < 0.05$).

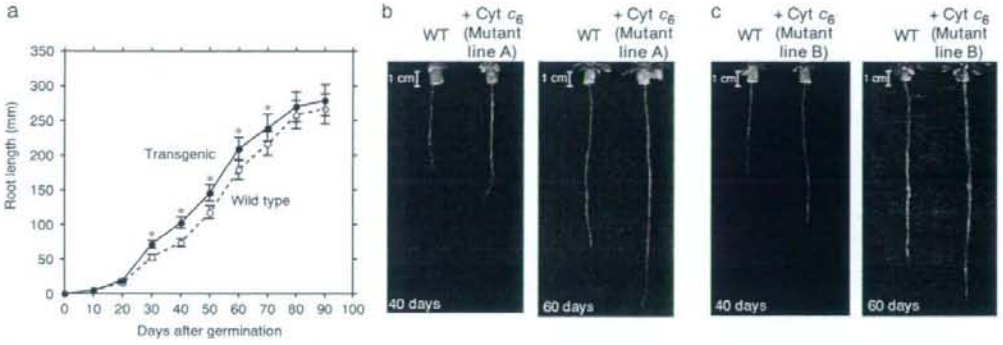

Fig. 4 Development of root lengths. (a) Time courses of root lengths of wild-type (open circles) and transgenic (filled circles) plants (mutant line A). (b) Root lengths of wild-type and transgenic *Arabidopsis* plants of mutant line A were photographed after 40 and 60 d. (c) Root lengths of wild-type and transgenic *Arabidopsis* plants of mutant line B were photographed after 40 and 60 d. The bars and asterisks have the same meaning as those in Fig. 3.

Moreover, there were no significant differences in plant height, leaf and root lengths between the mutant lines A and B. The average total numbers of flowers per plant were 60 ± 2 for the wild-type *Arabidopsis* and 62 ± 3 for the transgenic plants, showing no difference between the wild-type and transgenic plants. Flowering occurred 50 d after planting in the wild-type plants, whereas it occurred >7–12 d earlier in the transgenic plants (data not shown). These results indicate that the expression of *Porphyra* Cyt c_6 in *A. thaliana* promotes the growth of plants in the early stages.

Transgenic Arabidopsis with the Cyt c_6 gene shows higher amounts of metabolites

To investigate whether the amount of metabolites in transgenic plants increased in comparison with that in wild-type plants, we measured the amounts of chlorophylls, proteins, ATP, NADPH and starch. All experiments were carried out every 10 d from 30 to 80 d after planting, using eight wild-type and transgenic plants (mutant line A) at 3 h after illumination. Chlorophyll content in the transgenic plants expressing Cyt c_6 was 1.1- to 1.3-fold higher than that of wild-type plants (significant in t-test, $P<0.05$) (Fig. 5a). Concomitantly, the protein content of the transgenic plants was also significantly higher than that in the wild-type plants (t-test, $P<0.05$) (Fig. 5b). The contents of ATP, NADPH and starch were also higher in the transgenic plants from 40 to 80 d after planting (Fig. 5c, d, e). For example, 60 d after planting, in the transformants, the amounts of protein, ATP, NADPH and starch were 1.1-, 1.9-, 1.4- and 1.2-fold those in the wild-type plants, respectively. The results clearly indicate that the larger plant body of the transgenic plants is not the result of succulent growth, but is the consequence of substantial growth.

Expression of Porphyra Cyt c_6 enhances photosynthesis in Arabidopsis

The capacity for CO_2 assimilation, which uses ATP and NADPH produced by photosynthetic electron transfer and photophosphorylation (Schurmann et al. 1971, Arnon 1984), was determined with the plants grown for 60 d after planting, which had fully developed leaves suitable for the measurements. The CO_2 assimilation capacity of the wild-type and the transgenic plants (mutant line A) was 1.420 ± 0.091 and 1.862 ± 0.304 μmol $CO_2\,m^{-2}\,s^{-1}$, respectively. The differences were also observed in plants grown for 70 or 80 d after planting, and were statistically significant (t-test, $P<0.05$).

To investigate the cause of enhanced photosynthesis in transgenic plants expressing Cyt c_6, we determined photosynthetic parameters by measuring chlorophyll fluorescence under growth light conditions using mutant line A plants (Table 1). The parameter Φ_{PSII}, which reflects effective quantum yields of photosynthesis, was somewhat higher in the transgenic plants, confirming that the expression of Cyt c_6 enhances photosynthesis. The increased quantum yield of photosynthesis must be due to either the increase of the quantum yield of open PSII (reflected in the parameter F_v'/F_m') or the decrease of excitation pressure $1-qP$, which reflects the redox state of the plastoquinone pool of the photosynthetic electron transport system. F_v'/F_m', together with F_v/F_m, the maximum quantum yield of PSII, did not show any significant difference between wild-type and transgenic plants. On the other hand, $1-qP$ is lower in the transgenic plants by 30%, suggesting that the

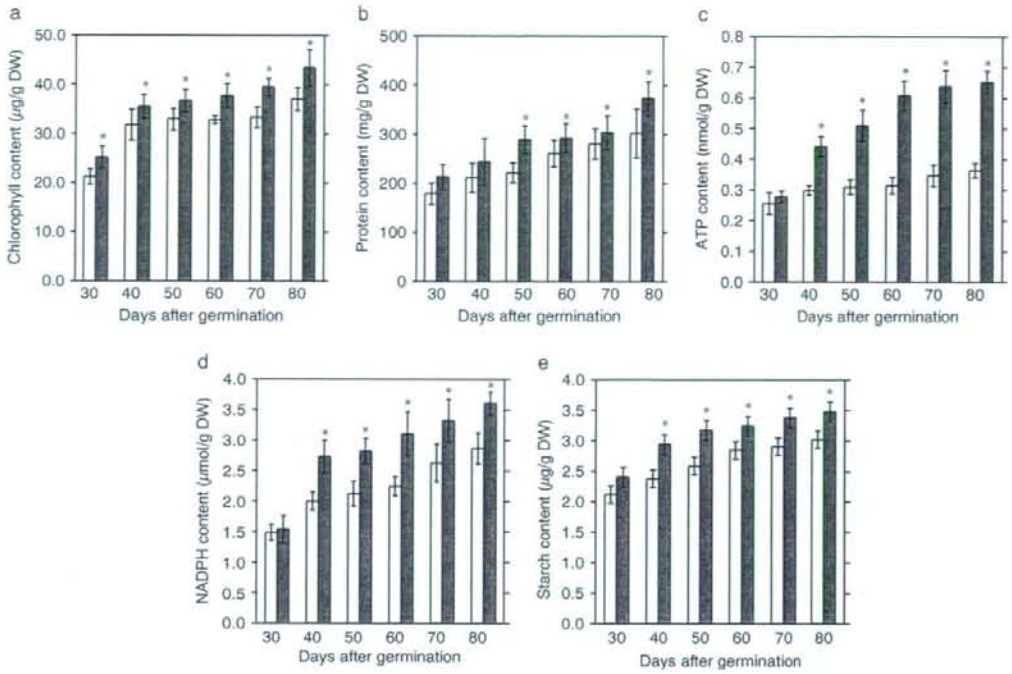

Fig. 5 Comparison of the amount of metabolites between wild-type and transgenic plants grown for 30, 40, 50, 60, 70 and 80 d, 3 h after illumination. (a) The content of chlorophylls. (b) The content of proteins. (c) The content of ATP. (d) The content of NADPH. (e) The content of starch. Data are the means ± SD of eight plants in each experiment. The bars correspond to the SD from eight plants in each experiment. White and gray boxes indicate wild-type and transgenic plants, respectively. Asterisks indicate that the difference between the wild-type and transgenic plants was significant by a *t*-test ($P<0.05$).

Table 1 Fluorescence characteristics of wild-type and transgenic plants

	Wild-type	Transgenic
$1-qP$	0.060 ± 0.0072	0.042 ± 0.0020
Φ_{PSII}	0.699 ± 0.0168	0.716 ± 0.0077
F_v/F_m	0.793 ± 0.0121	0.793 ± 0.0081
F'_v/F'_m	0.744 ± 0.0125	0.748 ± 0.0090
qN	0.195 ± 0.0275	0.194 ± 0.0348

The values represent the mean ± SD, which was calculated for three independent measurements. Minimum chlorophyll fluorescence (F_o) was determined by applying the measuring light (650 nm) at 0.02 μmol photons $m^{-2} s^{-1}$. A saturating pulse of white light at 2,600 μmol $m^{-2} s^{-1}$ set for 0.8 s from a light source (KL 1500; Schott, Wiesbaden, Germany) was applied to determine the maximum chlorophyll fluorescence in the dark (F_m) and that during actinic light illumination (F'_m). The steady state of chlorophyll fluorescence (F) was recorded during actinic illumination (50 μmol photons $m^{-2} s^{-1}$).

plastoquinone pool is more oxidized in the transgenic plants (*t*-test, $P<0.05$). These results indicate that an increase in the efficiency of photosynthetic electron transport is due to more efficient electron transfer downstream of the plastoquinone pool, but not to the change in PSII reaction center complexes. The parameter qN, which reflects non-photochemical quenching of chlorophyll fluorescence, did not show any difference between wild-type and transgenic plants.

Discussion

Confirmation of electron transfer of Porphyra Cyt c_6 to Arabidopsis PSI in vitro

In vitro experiments first demonstrate that Cyt c_6 from the red alga *P. yezoensis* can transfer an electron to *Arabidopsis* PSI, and the half-life (time) of *Arabidopsis* PSI reduction of *Porphyra* Cyt c_6 was shorter than that of

Arabidopsis PC (Fig. 1). Likewise, in the cyanobacteria *Pseudanabaena* sp. PCC6903, the half-life (time) of *Pseudanabaena* PSI of Cyt c_6 was shorter than that of PC (Hervás et al. 1998). It has been suggested that release of oxidized PC from PSI limits electron transfer between Cyt b_6f and PSI (Finazzi et al. 2005). The shorter half-life (time) of the dark reduction kinetics of *Arabidopsis* PSI by *Porphyra* Cyt c_6 compared with *Arabidopsis* PC (Fig. 1) could be attributed to faster release of oxidized *Porphyra* Cyt c_6 from *Arabidopsis* PSI compared with *Arabidopsis* PC, since our excitation flash is not single-turnover for the PSI reaction center.

Introducing the Porphyra Cyt c_6 gene into Arabidopsis would accelerate growth and the amounts of metabolites of plants

We next introduced *Porphyra* Cyt c_6 into the model plant *A. thaliana* (Fig. 2a–d). This is the first report on the expression of *Porphyra* Cyt c_6 in *A. thaliana* chloroplasts. Then, we found that reinforcement of photosynthetic electron transfer and photophosphorylation is caused by introducing the *Porphyra* Cyt c_6 gene into the model plant *A. thaliana*. The *Arabidopsis* expressing *Porphyra* Cyt c_6 not only enhances growth measured in terms of plant height, and leaf and root lengths, but also increases the amount of chlorophylls, proteins, ATP, NADPH and starch (Figs. 3–5). The increasing rate of photosynthesis in transgenic plants thus could lead to an increase in ATP and NADPH, which are products of photosynthetic electron transfer and photophosphorylation, and universal energy currencies of living cells. In addition, since glutamine synthase, which plays pivotal roles in the biosynthesis of amino acids, catalyzes the ATP-dependent amination of glutamate to glutamine in plants (Temple et al. 1998), an increase in ATP levels of the transgenic plants may contribute to enhancement of the biosynthesis of amino acids and proteins. The content of starch and the CO_2 assimilation capacity of transgenic plants should be enhanced since the increased contents of ATP and NADPH may be used for starch synthesis (Stark et al. 1992) and the Calvin–Benson cycle. Furthermore, the Cyt c_{6A} of higher plants cannot complement the PC-null *Arabidopsis* mutant phenotype (Weigel et al. 2003). Our results show that the algal Cyt c_6 transfers the electron directly to *Arabidopsis* PSI in vitro (Fig. 1). Accordingly, introduction of the algal Cyt c_6 into *A. thaliana* should be possible to complement the PC-null *Arabidopsis* mutant. This is a very interesting subject worthy of further study.

Expression of Porphyra Cyt c_6 enhances photosynthetic electron transfer in Arabidopsis

Analysis of chlorophyll fluorescence indicates that the rate of linear electron transport in the steady state is enhanced in transgenic plants, compared with that in wild-type plants, and the plastoquinone pool ($1 - qP$) is more oxidized in transgenic *A. thaliana* plants than in the wild-type plants (Table 1). Generally, the rate-limiting step of the photosynthetic electron transport system is considered to be the electron transfer between reduced plastoquinone and Cyt b_6f (Junge 1977). However, the expression of Cyt c_6, which is located downstream of Cyt b_6f in photosynthetic electron transport, appears to lead to an increase in electron transfer efficiency. It was reported that an increase in the relative amount of PSI led to an increase in the rate of overall electron transfer in photosynthesis in the cyanobacterium *Synechococcus* sp. PCC6803 (Sonoike et al. 2001). This indicates that the enhancement of photosynthetic electron transfer could be realized by the increase in the rate of electron transfer even if it is not the rate-limiting step. The transgenic plants exhibited a higher Φ_{PSII} than that in the wild-type plants. The difference would be large enough to enhance the growth and increase the amounts of chlorophylls, proteins and metabolites such as ATP and NADPH, probably because the increase in electron transfer efficiency in the transgenic plants accumulates continuously during the entire growth period of the plants. Since the molar content of Cyt c_6 in the transgenic plants is estimated as 1.2-fold that of PC, the total amount of electron donor to PSI in the transgenic plants should be more than twice that in wild-type plants, suggesting that this increase may primarily contribute to the increased rate of photosynthesis in the transgenic plants. Intrinsic PC is also expressed in transgenic *Arabidopsis* plants. Intrinsic PC with higher affinity for PSI may compete with introduced Cyt c_6 with lower affinity. Therefore, it is possible that the expression of Cyt c_6 in PC-null *Arabidopsis* mutants would further enhance not only photosynthetic electron transfer but also growth and the amounts of the metabolites.

Here we show that the enhancement of photosynthesis, metabolites and growth of the model plant *A. thaliana* could be realized by expressing the gene of a protein that functions in photosynthetic electron transport of the components of the light reaction.

Materials and Methods

Protein purification and flash-induced kinetic analysis in vitro

Cyt c_6 from the red alga *P. yezoensis* was purified according to the method previously reported (Yamada et al. 2000, Satoh et al. 2002). The PC from *A. thaliana* was the recombinant protein expressed in *Escherichia coli* according to previous reports (Lange et al. 2005) with slight modifications. The isolation of PSI from *A. thaliana* was carried out as described, according to the method of Hiyama (2004). The chlorophyll concentration of *A. thaliana* PSI was determined by the method of Mackinney (1941). Flash-induced absorption changes of P700 of PSI were monitored by a pulse amplitude-modulated system (PAM 101/102, Walz, Effeltrich, Germany) with a dual wavelength emitter/detector

unit (EDP700DW-E, Walz). Excitation flash was provided by a xenon flash (XE-STL, Walz) with a control unit (XE-STC, Walz); at the highest flash intensity, the width of the flash is 1.5 µs at the half-maximal intensity. Output signals were digitized and analyzed by a 12-bit A/D converter (AXP-AD02, Adtek System Science Co. Ltd, Japan) with a laboratory-made program. Reaction medium contained 20 mM HEPES (pH 7.0), 0.03% dodecyl maltoside, 2 mM methyl viologen, 10 mM sodium ascorbate, 5 mM $MgCl_2$ and PSI preparations containing 10 µg chlorophyll ml^{-1} and 1, 2, 5, 10, 15 and 20 µM of *Porphyra* Cyt c_6 or *Arabidopsis* PC, respectively. All the measurements were carried out at room temperature (25°C).

Plant material and growth conditions

Arabidopsis thaliana ecotype Columbia (Col-0) was used for all experiments. Plants were grown under controlled light conditions (50 µmol photons $m^{-2}s^{-1}$) in a 16 h light/8 h dark cycle at 20–22°C at relative air humidity of 60–70%.

Transgenic Arabidopsis

The gene encoding mature Cyt c_6 peptides (Satoh et al. 2002) was amplified from the genomic DNA of *P. yezoensis* by PCR using specific primers (i.e. Pyc61, 5′-CCGCGGAGACGTTAAA TTGAAGAAGAAGC-3′ and Pyc62, 5′-GGAGCTCTTACCAAC CTTTTTCAGATTGAG-3′). The *petE* transit peptides were acquired from *A. thaliana* (Theologis et al. 2000) by PCR using specific primers (AtPcsig1, 5′-GGATCCATGGCCGCAATTACA TCAGCTACCG-3′ and AtPcsig2, 5′-TGCACTGCAGCCATCG CATTTCAGCTAAAACG-3′). Amplified DNA fragments were cleaved using the *Pst* I enzyme. The cleaved DNA fragments were ligated. The constructed DNA fragments (encoding *P. yezoensis* Cyt c_6 mature peptides with *A. thaliana petE* transit peptides) were restricted by *Bam*HI and *Sac*I, and inserted in between the cauliflower mosaic virus 35S promoter and the *nos* transcriptional terminator of the pBI121 binary vector. The constructed plasmids were introduced into the *Agrobacterium tumefaciens* strain LBA4404 by triparental mating and then into *Arabidopsis* plants by vacuum infiltration (Dandekar et al. 2005).

Thermal asymmetric interlaced (TAIL)-PCR

Total DNA was extracted from the mutant plant for TAIL-PCR (Liu et al. 1995, Liu et al. 2005). Primers specific to the T-DNA left borders were LB1 (5′-TTCGCCCTTTGACGTTGG AGTCCACG-3′), LB2 (5′-GTTCCAAACTGGAACAACACTC AACC-3′) and LB3 (5′-GGATTTTGCCGATTTCGGAACC ACC-3′). The degenerate primers used were AD1 (5′-NTCGA STWTSGWGTT-3′), AD2 (5′-NGACGASWGANAWGAA-3′) and AD3 (5′-NGTAWAASGTNTSCAA-3′). After tertiary PCR, fragments were separated by gel electrophoresis and purified from gels. Purified fragments were directly sequenced.

Introduction and expression analysis

Total DNA and RNA were isolated from whole leaves of 4-week-old plants using Isoplant II (Nippon Gene Co. Ltd, Japan) and an RNeasy Plant mini kit (Qiagen K.K., Tokyo, Japan), respectively. Polyadenylated RNA was isolated from 100 µg of total RNA using oligo(dT)-cellulose according to the Oligotex™-dT30 (Super) mRNA purification kit manual (Takara Shuzo Co. Ltd, Japan). The introduced Cyt c_6 gene was confirmed using PCR. The expression of Cyt c_6 mRNA was verified by RT–PCR. For Western blot analysis, intact chloroplasts were separated from whole leaves of 6-week-old plants using a Percoll buoyant density gradient (Robinson 1983), and chloroplast protein was extracted, separated by SDS–PAGE and transferred onto a nitrocellulose membrane for antibody probing. The level of PC was determined as described previously (Kieselbach et al. 1998, Navarro et al. 2004).

Growth experiments

The height of the plants was measured from the stem tip to the base of the hypocotyl. Root length was measured from the root tip to the base of the hypocotyls, and the length of leaves was recorded.

Determination of chlorophyll, protein and metabolites

Chlorophyll was extracted from a fully expanded leaf using 80% acetone. Total chlorophyll content was determined according to the method of Mackinney (1941). Total proteins were extracted using CelLytic P (Sigma Aldrich JAPAN K.K., Tokyo, Japan) and determined using the Lowry method (Lowry et al. 1951). The content of ATP was determined by luciferin–luciferase assay (Larsson and Olsson 1979) using GENE LIGHT 55 (Microtech Co. Ltd, Japan). The content of NADPH was measured as described by Häusler et al. (2000) and content of starch was measured as described by Leegood (1993).

CO_2 assimilation measurement

The CO_2 assimilation rate was determined using a portable CO_2 gas analyzer (CIRAS-1; Koito Industries, Ltd, Japan) using individual rosette leaves of 60-, 70- and 80-day-old plants during the first 3 h of the photoperiod. The measurement was carried out under conditions of 350 p.p.m. CO_2 and a constant irradiance of 1,500 µmol photons $m^{-2}s^{-1}$ on the upper surface of the leaves.

Chlorophyll fluorescence measurement

Chlorophyll fluorescence was measured using a PAM fluorometer (Waltz) with the emitter/detector unit ED101 as described previously (Schreiber 1986). Rosettes from each plant were dark adapted for 10 min before measurement. Minimum chlorophyll fluorescence (F_o) was determined by applying the measuring light (650 nm) at 0.02 µmol photons $m^{-2}s^{-1}$. A saturating pulse of white light at 2,600 µmol $m^{-2}s^{-1}$ set for 0.8 s from a light source (KL 1500; Schott, Wiesbaden, Germany) was applied to determine maximum chlorophyll fluorescence in the dark (F_m) and that during actinic light illumination (F'_m). The steady state of chlorophyll fluorescence (F) was recorded during actinic illumination (50 µmol photons $m^{-2}s^{-1}$). The maximum quantum yield of PSII (F_v/F_m) and the quantum yield of open PSII under actinic illumination (F'_v/F'_m) were calculated as $(F_m - F_o)/F_m$ and $((F'_m - F'_o)/F'_m$, respectively. Excitation pressure $(1 - qP)$, which reflects the reduced state of the plastoquinone pool, was calculated using $1 - (F'_m - F)/(F'_m - F_o)$. Non-photochemical quenching (qN) and the effective quantum yield of electron transfer (Φ_{PSII}) were calculated using $1 - [(F'_m - F'_o)/(F_m - F_o)]$ and $(F'_m - F)/F'_m$, respectively. Difference was calculated as (transgenic − wild type)/wild type × 100 (%).

Data analysis

Data analysis and calculations were carried out using Microsoft Excel (Microsoft Corporation, Redmond, USA). Statistically significant differences between the plants with altered Cyt c_6 expression and the wild-type control were analyzed using Student's t-test ($P < 0.05$). Data are shown as means ± SD.

Acknowledgments

Arabidopsis thaliana Col-0 seeds were kindly provided by Professor S. Naitoh (Hokkaido University). We thank Dr. C. Fukazawa for providing the binary vector pBI121 and *A. tumefaciens*. The red alga *P. yezoensis* was a gift from Shirako Co. Ltd. We are indebted to S. Tanaka, S. Fukuzawa, T. Kikuchi, S. Nagata, K. Matsuoka, M. Matsuda, H. Nakade, K. Hoshikawa, T. Endo, Y. Katoh, I. Shirasaki and M. Hirayama for cultivating the plants. CO_2 assimilation measurement was performed according to the instructions of Dr. K. Ujiie. This work was supported in part by a Grant-in-Aid for Scientific Research (C) and for the 21st Century's Center of Excellence (COE) program from the Ministry of Education, Culture, Sports, Science and Technology of Japan.

References

Arnon, D.I. (1984) The discovery of photosynthetic phosphorylation. *Trends Biochem. Sci.* 9: 258–262.

Chida, H., Yokoyama, T., Kawai, F., Nakazawa, A., Akazaki, H., et al. (2006) Crystal structure of oxidized cytochrome c_{6A} from *Arabidopsis thaliana*. *FEBS Lett.* 580: 3763–3768.

Dandekar, A. and Fisk, H.J. (2005) Plant transformation. Agrobacterium-mediated gene transfer. *Methods Mol. Biol.* 286: 35–46.

De la Rosa, M.A., Navarro, J.A., Diaz-Quintana, A., De la Cerda, B., Molina-Heredia, F.P., et al. (2002) An evolutionary analysis of the reaction mechanisms of photosystem I reduction by cytochrome c_6 and plastocyanin. *Bioelectrochemistry* 55: 41–45.

De la Rosa, M.A., Molina-Heredia, F.P., Hervás, M. and Navarro, J.A. (2006) Convergent evolution of cytochrome c_6 and plastocyan. *In* Photosystem I: The Light-Driven Plastocyanin. Edited by Golbeck, J.H. pp. 683–696. Springer, The Netherlands.

Finazzi, G., Sommer, F. and Hippler, M. (2005) Release of oxidized plastocyanin from photosystem I limits electron transfer between photosystem I and cytochrome b_6f complex in vivo. *Proc. Natl Acad. Sci. USA* 102: 7031–7036.

Gupta, R., He, Z. and Luan, S. (2002) Functional relationship of cytochrome c_6 and plastocyanin in *Arabidopsis*. *Nature* 417: 567–571.

Hageman, J., Robinson, C., Smeekens, S. and Weisbeek, P. (1986) A thylakoid processing protease is required for complete maturation of the lumen protein plastocyanin. *Nature* 324: 567–569.

Häusler, R.E., Fischer, K.L. and Flügge, U.F. (2000) Determination of low-abundant metabolites in plant extracts by NAD(P)H fluorescence with a microtiter plate reader. *Anal. Biochem.* 281: 1–8.

Hervás, M., Navarro, J.A., Molina-Heredia, F.P. and De la Rosa, M.A. (1998) The reaction mechanism of photosystem I reduction by plastocyanin and cytochrome c_6 follows two different kinetic models in the cyanobacterium *Pseudanabaena* sp. PCC 6903. *Photosynth. Res.* 57: 93–100.

Hervás, M., Ortega, J.M., Navarro, J.A., De la Rosa, M.A. and Bottin, H. (1994) Laser flash kinetic analysis of *Synechocystis* PCC 6803 cytochrome c_6 and plastocyanin oxidation by photosystem I. *Biochim. Biophys. Acta* 1184: 235–241.

Hiyama, T. (2004) Isolation of photosysystem I particles from spinach. *Methods Mol. Biol.* 274: 11–17.

Howe, C.J., Schlarb-Ridley, B.G., Wastl, J., Purton, S. and Bendall, D.S. (2006) The novel cytochrome c_6 of chloroplasts: a case of evolutionary *bricolage*? *J. Exp. Bot.* 57: 13–22.

Junge, W. (1977) Physical aspects of light harvesting, electron transport and electrochemical potential generation in photosynthesis of green plants. *In* Encyclopedia of Plant Physiology Vol. 5: Photosynthesis. Edited by Trebst, A. and Avron, M. pp. 59–93. Springer-Verlag, New York.

Katoh, S. (1960a) Crystallization of an algal cytochrome, *Porphyra tenera*-cytochrome 553. *Nature* 186: 138–139.

Katoh, S. (1960b) A new copper protein from *Chlorella ellipsoidea*. *Nature* 186: 533–534.

Katoh, S. and Takamiya, A. (1961) A new leaf copper protein 'plastocyanin', a natural Hill oxidant. *Nature* 189: 665–666.

Kerfeld, C.A. and Krogman, D.W. (1998) Photosynthetic cytochromes *c* in cyanobacteria, algae and plants. *Annu. Rev. Plant Physiol. Plant Mol. Biol.* 49: 397–425.

Kieselbach, T., Hagman, Å., Anderson, B. and Schröder, W.P. (1998) The thylakoid lumen of chloroplasts. *J. Biol. Chem.* 273: 6710–6716.

Ku, M.S., Agarie, S., Nomura, M., Fukayama, H., Tsuchida, H., et al. (1999) High-level expression of maize phosphoenolpyruvate carboxylase in transgenic rice plants. *Nat. Biotechnol.* 17: 76–80.

Lange, C., Cornvik, T., Diaz-Moleno, I. and Ubbink, M. (2005) The transient complex of poplar plastocyanin with cytochrome *f*: effects of ionic strength and pH. *Biochim. Biophys. Acta* 1707: 179–188.

Larsson, C.M. and Olsson, T. (1979) Firefly assay of adenine nucleotides from algae: comparison of extraction methods. *Plant Cell Physiol.* 20: 145–155.

Leegood, R.C. (1993) Carbon metabolism. *In* Photosynthesis and Production in a Changing Environment: A Field and Laboratory Manual. Edited by Hall, D.O., Scurlock, J.M.O., Bolhàr-Nordenkampf, R.C., Leegood, R.C. and Long, S.P. pp. 247–267. Chapman and Hall, London.

Liu, Y.G., Chen, Y. and Zhang, Q. (2005) Amplification of genomic sequences flanking T-DNA insertions by thermal asymmetric interlaced polymerase chain reaction. *Methods Mol. Biol.* 286: 341–348.

Liu, Y.G., Mitsukawa, N., Oosumi, T. and Whittier, R.F. (1995) Efficient isolation and mapping of *Arabidopsis thaliana* T-DNA insert junctions by thermal asymmetric interlaced PCR. *Plant J.* 8: 457–463.

Lowry, O.H., Rosebrough, N.J., Farr, A.L. and Randall, R.J. (1951) Protein measurement with the folin phenol reagent. *J. Biol. Chem.* 193: 265–275.

Mackinney, G. (1941) Absorption of light by chlorophyll solutions. *J. Biol. Chem.* 140: 315–322.

Merchant, S. and Bogorad, L. (1987) The Cu(II)-repressible plastidic cytochrome *c*: cloning and sequence of a complementary DNA for the pre-apoprotein. *EMBO J.* 6: 2531–2535.

Miyagawa, Y., Tamoi, M. and Shigeoka, S. (2001) Overexpression of a cyanobacterial fructose-1,6-/sedoheptulose-1,7-bisphosphatase in tobacco enhances photosynthesis and growth. *Nat. Biotechnol.* 19: 965–969.

Molina-Heredia, F.P., Wastl, J., Navarro, J.A., Bendall, D.S., Hervás, M., et al. (2003) A new function for an old cytochrome? *Nature* 424: 33–34.

Navarro, J.A., Hervás, M. and De la Rosa, M.A. (2004) Purification of plastocyanin and cytochrome c_6 from plants, green algae and cyanobacteria. *Methods Mol. Biol.* 274: 79–92.

Rodriguez, R.E., Lodeyro, A., Poli, H.O., Zurbriggen, M., Peisker, M., Palatnik, J.F., et al. (2007) Transgenic tobacco plants overexpressing chloroplastic ferredoxin-NADP(H) reductase display normal rates of photosynthesis and increased tolerance to oxidative stress. *Plant Physiol.* 143: 639–649.

Robinson, S.P. (1983) Isolation of intact chloroplasts with high CO_2 fixation capacity from sugar beet leaves containing calcium oxalate. *Photosynth. Res.* 4: 281–287.

Satoh, T., Itoga, A., Isogai, Y., Kurihara, M., Yamada, S., et al. (2002) Increasing the conformational stability by replacement of heme axial ligand in *c*-type cytochrome. *FEBS Lett.* 531: 543–547.

Schurmann, P., Buchanan, B.B. and Arnon, D.I. (1971) Role of cyclic photophosphorylation in photosynthetic carbon dioxide assimilation by isolated chloroplasts. *Biochim. Biophys. Acta* 267: 111–124.

Schreiber, U. (1986) Detection of rapid induction kinetics with a new type high-frequency modulated chlorophyll fluorometer. *Photosynth. Res.* 9: 261–272.

Sigfridsson, K. (1998) Plastocyanin, an electron-transfer protein. *Photosynth. Res.* 57: 1–28.

Soll, J. and Schleiff, E. (2004) Protein import into chloroplasts. *Nat. Rev. Cell. Biol.* 5: 198–208.

Sonoike, K., Hihara, Y. and Ikeuchi, M. (2001) Physiological significance of the regulation of photosystem stoichiometry upon high light

acclimation of *Synechocystis* sp. PCC6803. *Plant Cell Physiol.* 42: 379–384.

Stark, D.M., Timmerman, K.P., Barry, G.F., Preiss, J. and Kishore, G.M. (1992) Regulation of the amount of starch in plant tissues by ADP-glucose pyrophosphorylase. *Science* 9: 287–292.

Temple, S.J., Vance, C.P. and Gantt, J.S. (1998) Glutamate synthase and nitrogen assimilation. *Trends Plant Sci.* 3: 51–56.

Theologis, A., Ecker, J.R., Palm, C.J., Federspiel, N.A., Kaul, S., et al. (2000) Sequence and analysis of chromosome 1 of the plant *Arabidopsis thaliana*. *Nature* 408: 816–820.

Ullmann, G.M., Hauswald, M., Jensen, A., Kostic, N.M. and Knapp, E.W. (1997) Comparison of the physiologically equivalent proteins cytochrome c_6 and plastocyanin on the basis of their electrostatic potentials. Tryptophan 63 in cytochrome c_6 may be isofunctional with tyrosine 83 in plastocyanin. *Biochemistry* 36: 16187–16196.

Wastl, J., Bendal, D.S. and Howe, C. (2002) Higher plants contain a modified cytochrome c_6. *Trends Plant Sci.* 7: 244–245.

Weigel, M., Varotto, C., Pesaresi, P., Finazzi, G., Rappaport, F., et al. (2003) Plastocyanin is indispensable for photosynthetic electron flow in *Arabidopsis thaliana*. *J. Biol. Chem.* 278: 31286–31289.

Yamada, S., Park, S.Y., Shimizu, H., Koshizuka, Y., Kadokura, K., et al. (2000) Structure of cytochrome c_6 from the red alga *Porphyra yezoensis* at 1.57 Å resolution. *Acta Crystallogr. D* 56: 1577–1582.

(Received March 7, 2007; Accepted May 15, 2007)

Nucleic Acids Symposium Series No. 51 269–270
doi:10.1093/nass/nrm135

Recognition of longer duplex DNA by cooperative strand invasion

Toru Sugiyama[1*], Yasutada Imamura[2], Masaaki Kurihara[3], and Atsushi Kittaka[4]
[1]Department of Life Sciences, Graduate School of Arts and Sciences, The University of Tokyo, 3-8-1 Komaba, Meguro-ku, Tokyo 153-8902, Japan, [2]Faculty of Engineering, Kogakuin University, 2665-1 Nakano, Hachioji, Tokyo 192-0015, Japan, [3]Division of Organic Chemistry, National Institute of Health Sciences, Kamiyoga, Setagaya-ku, Tokyo 158-8501, Japan, and [4]Faculty of Pharmaceutical Sciences, Teikyo University, Sagamiko, Kanagawa 199-0195, Japan.

ABSTRACT

Peptide nucleic acid is a synthetic DNA mimic in which the sugar-phosphate backbone has been replaced by a peptide backbone. A remarkable feature of PNA is its ability to recognize sequences within duplex DNA by strand invasion. We have previously demonstrated that a PNA targeting six bases within duplex DNA cooperatively binds to 12 base-pair site by strand invasion. We here report an successful extension of the target site size to 18 base pairs without the expense of specificity.

INTRODUCTION

Sequence-specific recognition of double helical DNA is crucial to functional genomics, disease diagnosis, and human gene therapy. A variety of agents are available for specific targeting of predetermined DNA sequences including engineered zinc finger proteins, synthetic polyamides, triplex forming oligonucleotides (TFOs), and peptide nucleic acids (PNAs). Among them, of particular interest is strand invasion by PNA. PNA is one of the most successful analogues of oligonucleotides with potential applications in antisense and antigene strategy.[1)] Strand invasion can occur via several distinct mechanisms: triplex invasion,[1)] double-duplex invasion,[2)] and duplex invasion.[3,4)] Most studies have focused on triplex invasion by using homopyrimidine PNAs, because a number of oligonucleotide-dependent enzymatic reactions are inhibited by PNA, including restriction enzyme cleavage, transcription, and translation.

Figure 1. Schematic representation of triple cooperative strand invasion of dsDNA by PNA.

However, there remains considerable room for further investigations. One major challenge is recognition of a unique site in the human genome. This requires discrimination of a specific sequence of 15-16 base pairs from all other possible sequences. However, the affinity of relatively short bis-PNAs (8-10 bases) to their target sites is so high that PNA binding to correct and even to mismatched sites is virtually irreversible. In this regard, sequence-specificity of PNA triplex invasion is limited and this limitation hinders its application in living cells.

The specificity of DNA recognition can be improved by cooperative binding of two ligands to a target site. Cooperative interactions between DNA binding ligands are critical to their affinity and specificity. Many DNA-binding proteins rely on dimerization of DNA recognition elements that each occupy 4-6 base pairs and target unique contiguous sites in genomic DNA.

We have previously demonstrated that a short hexameric bis-PNA (PNA **1**) cooperatively invades into double-stranded DNA with excellent sequence specificity, discerning a single-base mismatch within a 12 base-paired target.[5)] We here report an extension of this idea to highly specific recognition of longer duplex DNA (Figure 1).

RESULTS AND DISCUSSION

We intend to extend the site size of DNA targets from 12 to 18 base pairs. As a straightforward approach, we tested triple tandem strand invasion of bis-PNAs. To avoid the complexity arising from various intermediate species, we used two different hexameric bis-PNAs, PNA **1** and PNA **2**. The purine target sequence 5'-$A_5GA_2GAGA_6G$-3' can be considered as three contiguous target sites, 5'-A_5G-3',5'-A_2GAGA-3', and 5'-A_5G-3'. Bis-PNAs were tested for cooperative strand invasion by the gel mobility shift assay.

PNA 1

H-Cys(SBu^t)-eg-TTTTTC-Lys$_3$-eg$_3$-CTTTTT-eg-Cys(SBu^t)Lys-CONH$_2$

PNA 2

H-Cys(SBu^t)-eg-TTCTCT-Lys$_3$-eg$_3$-TCTCTT-CONH$_2$

DNA D^T

3'——TTTTTC TTCTCT TTTTTC——5'
5'——AAAAAG AAGAGA AAAAAG——3'

DNA D^{T}mis

3'——TTTTTC TTCGCT TTTTTC——5'
5'——AAAAAG AAGCGA AAAAAG——3'

Figure 2. The sequences of PNA and DNA used in this study.

PNAs (Figure 2) were prepared by solid phase synthesis using standard Fmoc chemistry, then purified by HPLC, and characterized by MALDI-TOF mass spectrometry.

Combinations of PNA **1** and PNA **2** (2:1 ratio) were incubated at 25 °C with DNAs, 10 mM NaCl, 0.1% IGEPAL CA 630, 1 mM EDTA, and 10 mM sodium phosphate at pH 6.73. The reaction proceeded for 24 h and analyzed by polyacrylamide gel electrophoresis, followed by staining with ethidium bromide. Binding efficiency was quantitated by CCD-based densitometry of the individual bands.

Figure 3 shows the results of the gel mobility shift assay. PNA combinations incubated with D^T generated clear bands corresponding to triplex invasion complexes, indicating a positive binding interaction between contiguous PNAs, aligned head to tail in the invasion complex.

The sequence specificity was examined by comparing its affinity for fully matched 18 base pair target to that for a sequence containing a single-base mismatch (5'-AAAAAG AAGCGA AAAAAG-3'), D^{T}mis. Excellent specificity in an all-or-none manner was observed. Since each PNA molecule is bound to a short DNA target, a single mismatched base pair destabilizes such a complex to a large extent. This effect propagates to adjacent PNAs through conformational changes of double-stranded DNA, thus destabilizing the whole invasion complexes. Consequently, high specificity was achieved. A contiguous examination of cooperative strand invasion would overcome the problem of incorrect bindings that inevitably arises when targeting long DNA sequences. Further mechanistic investigations are currently in progress.

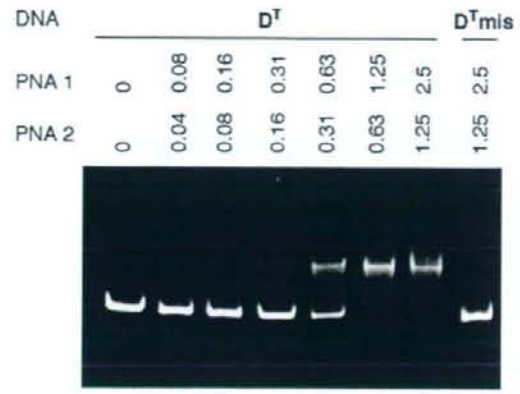

Figure 3. Polyacrylamide gel mobility shift assay showing binding at the PNA concentrations shown in μM to DNA D^T or D^{T}mis. Conditions: 10 mM sodium phosphate buffer, 1 mM EDTA (pH 6.73), 10 mM NaCl, 0.1% IGEPAL CA 630, 25°C.

CONCLUSION

We found a short bis-PNA cooperatively binds to three contiguous target sites within duplex DNA with excellent sequence specificity. This strategy would be useful to target a longer site and eventually enable the application of triplex invasion to antigene therapy.

REFERENCES

1. Nielsen, P. E., Egholm, M., Berg, R. H. and Buchard, O. (1991) *Science*, **254**, 1497-1500.
2. Lohse, J., Dahl, O. and Nielsen, P. E. (1999) *Proc. Natl. Acad. Sci. U.S.A.*, **96**, 11804-11808.
3. Nielsen, P. E. and Christensen, L. (1996) *J. Am. Chem. Soc.* **118**, 2287-2288.
4. Zhang, X., Ishihra, T. and Corey, D. R. (2000) *Nucleic Acids Res.*, **28**, 3332-3338.
5. Sugiyama, T, Imamura, Y., Hakamata, W., Kurihara, M. and Kittaka, A. (2006) *Nucleic Acids Symposium Series*, **50**, 157-158.

*Corresponding author. E-mail: csugi@mail.ecc.u-tokyo.ac.jp

Chem. Pharm. Bull. 55(5) 840—842 (2007) Vol. 55, No. 5

Controlling 3_{10}-Helix and -Helix of Short Peptides in the Solid State

Yosuke DEMIZU,[a] Masakazu TANAKA,*[,a] Masanobu NAGANO,[a] Masaaki KURIHARA,[b] Mitsunobu DOI,[c] Tokumi MARUYAMA,[d] and Hiroshi SUEMUNE*[,a]

[a] *Graduate School of Pharmaceutical Sciences, Kyushu University; 3–1–1 Maidashi, Higashi-ku, Fukuoka 812–8582, Japan:* [b] *Division of Organic Chemistry, National Institute of Health Sciences; Tokyo 158–8501, Japan:* [c] *Osaka University of Pharmaceutical Sciences; Osaka 569–1094, Japan: and* [d] *Faculty of Pharmaceutical Sciences at Kagawa Campus, Tokushima Bunri University; Kagawa 769–2193, Japan.*

Received December 17, 2006; accepted February 12, 2007

L-Leu hexapeptide containing -aminoisobutyric acid (Aib) forms a right-handed (*P*) 3_{10}-helix, whereas that containing cyclic , -disubstituted amino acid Ac_5c^{dOM} assumes a right-handed (*P*) -helix in the solid state.

Key words , -disubstituted amino acid; peptide; helix; conformation; secondary structure

-Aminoisobutyric acid (Aib; -methylalanine),[1—4] in which the -hydrogen atom of L-Ala is replaced with a methyl substituent, has strong propensity for helix formation and -sheet breaker. Thus Aib is widely used to construct helical structures, and to design drug candidates and organocatalysts.[3,4] Although the helical structure in proteins almost always is an -helix,[5] the tendency of Aib in short peptides is a 3_{10}-helix rather than an -helix. Furthermore, the Aib is an achiral amino acid, and thus does not have a bias for the helical-screw handedness. Over the last decade, chiral , -disubstituted -amino acids (dAAs) have been widely investigated.[6—9] However, the incorporation of chiral -methylated dAAs into peptides stabilizes the 3_{10}-helix, but not the -helix in short peptides. Moreover, it is believed that -helix formation usually requires a peptide having more than seven amino acid residues,[4,10,11] and the hexapeptide having dAA does not form the -helix, but assumes the 3_{10}-helix in the crystal state. Herein, we describe chiral cyclic dAA; 1-amino-3,4-dimethoxycyclopentanecarboxylic acid (Ac_5c^{dOM}), which has propensity for -helix formation, and the right-handed (*P*) -helix of its short Leu-hexapeptide.

We efficiently synthesized (*S*,*S*)-Ac_5c^{dOM} as previously reported,[12] and also the enantiomeric (*R*,*R*)-Ac_5c^{dOM} starting from dimethyl D-(−)-tartrate. Four L-Leu hexapeptides; Cbz-(L-Leu-L-Leu-dAA)$_2$-OMe [dAA=**1**: Aib; **2**: Ac_5c; **3**: (*S*,*S*)-Ac_5c^{dOM}; **4**: (*R*,*R*)-Ac_5c^{dOM}] were prepared by solution-phase methods.

At first, we studied the preferred conformation of **1**—**4** in $CDCl_3$ solution (1.0 mM) using FT-IR absorption spectroscopy. The IR spectra of **1**—**4** showed a weak band at 3430 cm^{-1} [free (solvated) peptide NH groups], and a strong band at 3340 cm^{-1} [intramolecularly H-bonded peptide NH groups]. These IR spectra are very similar to those of the reported helical Leu-peptides having Aib.[13]

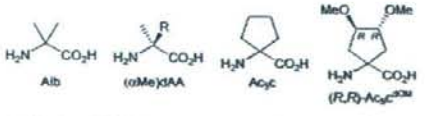

Fig. 1. Achiral and Chiral , -Disubstituted -Amino Acids

The ROESY or NOESY ^{1}H-NMR spectra did not clearly show the complete series of sequential d_{NN} cross-peaks of NOEs, which are characteristic of helical structures. Also, we could not discriminate between 3_{10}- and -helices of the Ac_5c^{dOM} peptides **3** and **4** because neither the $d_{N}(i, i+2)$ nor $d_{N}(i, i+4)$ (i=1 and 2) cross-peaks of NOEs were shown, or the relevant peaks were overlapped, whereas the $d_{N}(i, i+2)$ (i=1 and 2) cross-peaks of NOEs (typical peaks for the 3_{10}-helix) in the Aib peptide **1** were observed.

Figure 2 shows the CD spectra of **1**—**4** in 2,2,2-trifluoroethanol (TFE) solution, and also in the solid state (KCl disk). All these spectra show negative maxima at 222—228 and 204—208 nm and a positive maximum at 191—193 nm, which are characteristic of a right-handed (*P*) helical structure. The L-Leu residues in the peptides would control the helical-screw direction to the right-handedness.[13]

Judging from the ratio of R [maxima: $_{222}/_{208}$] in TFE solution, the Aib, Ac_5c, and (*R*,*R*)-Ac_5c^{dOM} peptides **1** (R=0.3), **2** (R=0.4), and **4** (R=0.4) might form a 3_{10}-helix and the (*S*,*S*)-Ac_5c^{dOM} peptide **3** (R=0.6) form a mixture of 3_{10}- and -helices. The CD spectra of Ac_5c^{dOM} hexapeptides in the solid state are distinct from those of the Aib and Ac_5c hexapeptides. The R values of the Ac_5c^{dOM} peptides **3** and **4** were 1.0, while those of the Aib and Ac_5c peptides **1** and **2** were 0.5 (red-shift of the maximum at 222 nm was observed). These R values mean that the Ac_5c^{dOM} hexapeptides form (*P*) -helices and the Aib and Ac_5c hexapeptides form (*P*) 3_{10}-helices.[14,15] The CD spectra of prototype Ac_5c (non-MeO-substituent) peptide are more similar to those of Aib peptides than those of Ac_5c^{dOM} peptides. These results validate the importance of the methoxy substituents, especially in terms of hydrophilicity and stereochemistry, on the cyclopentane ring for the -helix formation.

The crystal structures of Aib hexapeptide **1** and (*S*,*S*)-Ac_5c^{dOM} hexapeptide **3** were determined by X-ray crystallographic analysis as shown in Fig. 3.[16] As usual, in the crystal structure of the Aib peptide **1**, three consecutive hydrogen bonds of the $i \leftarrow i+3$ type, N(4)H···O=C(1) (N···O 3.20 Å; N–H···O 146.3°), N(5)H···O=C(2) (N···O 2.99 Å; N–H···O 159.5°), and N(6)H···O=C(3) (N···O 3.19 Å; N–H···O 149.4°) were observed, albeit the distance of N(3)H···O=C(0) (N···O 3.43 Å) is long for a hydrogen bond. The average , torsion angles are −66.1°, −31.3°, meaning the right-handed (*P*) 3_{10}-helix.[17] Contrary to the 3_{10}-helix of Aib peptide **1**, in the crystal structure of (*S*,*S*)-Ac_5c^{dOM} peptide **3**, two crystallographically independent molecules *A* and *B*, which are not 3_{10}-helices but right-handed (*P*) -helices (3.6_{13}-helices) exist, along with methanol and water molecules. In general, both molecules *A* and *B* are similar in the peptide backbone, but some differences at the side chain, the N-terminus protecting group, and especially at the C-terminal amino acid Ac_5c^{dOM} (6) and the L-Leu (5) were observed. The average , torsion angles are *A*: =−63.7°, =−40.4° and *B*: =−75.8°, =−28.4°, respectively.

Judging from the torsion angles, the molecule *B* seems to

* To whom correspondence should be addressed. e-mail: mtanaka@phar.kyushu-u.ac.jp; suemune@phar.kyushu-u.ac.jp

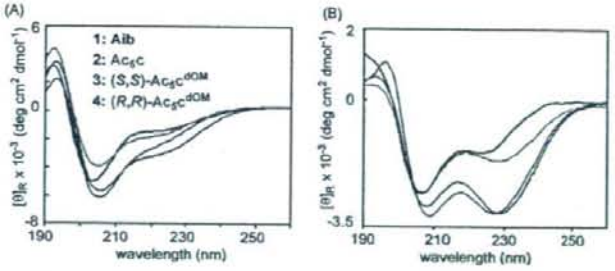

Fig. 2. CD Spectra of Leu-Hexapeptides

(A) Hexapeptides **1**—**4** in TFE solution; (B) **1**—**4** in KCl disk.

be a distorted (*P*) -helix, especially at the amino acid residues L-Leu (5) (=−99.6°, =−11.4°) and Ac_5c^{dOM} (6) (=+64.9°, =−167.0°). In the crystal state, two consecutive intramolecular hydrogen bonds of the *i*←*i*+4 type, N(5)H···O=C(1) (N···O 2.99 Å; N–H···O 150.4°) and N(6)H···O=C(2) (N···O 3.03 Å; N–H···O 151.1°) in the molecule *A*, and N(5)H···O=C(1) (N···O 2.91 Å; N–H···O 145.2°) and N(6)H···O=C(2) (N···O 2.98 Å; N–H···O 136.6°) in the molecule *B*, are found, respectively. The N···O distances (3.49, 3.76 Å) of N(4)H···O=C(0) in the molecules *A* and *B* are too long for a hydrogen bond. Interestingly, the (*S*,*S*)-Ac_5c^{dOM} peptide **3** crystallized to give two shapes of crystals: plates and needles. The latter seem to have different lattice parameters.

Molecular-mechanics calculation of the Ac_5c^{dOM} hexapeptides **3** and **4** with MacroModel produced right-handed (*P*) 3_{10}-helices as a global minimum-energy conformation, but not -helices.[18]

In conclusion, we have disclosed that the propensity of Ac_5c^{dOM} is an -helix formation, whereas that of Aib is a 3_{10}-helix formation. Although it is generally believed that the -helix formation usually needs a peptide composed of more than seven amino acid residues,[4,10,11] the L-Leu-hexapeptides containing Ac_5c^{dOM} assumed the right-handed (*P*) -helices in the crystal state. These peptides might be one of the shortest (*P*) -helical ones, albeit the 3_{10}/ -helical pentapeptide containing Aib has been reported.[19] The helicogenic property of (*S*,*S*)-Ac_5c^{dOM} is left-handed and that of enantiomeric (*R*,*R*)-Ac_5c^{dOM} is right-handed,[12] though their properties of helical handedness are weaker than that of L-Leu. The bulkiness, flexibility, and hydrophilicity of substituents at the cyclopentane ring would affect the secondary structures of their peptides, not only helical-screw handedness but also helical pitches (-helix or 3_{10}-helix).[12,20–22] Study of the detailed effect of substituents at the cyclopentane rings on the secondary structures is currently underway.

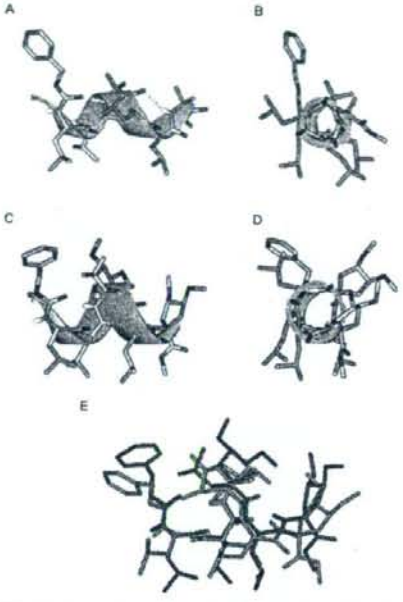

Fig. 3. Illustrative Structures Determined by X-Ray Crystallographic Analysis

(A), (B) Right-handed (*P*) 3_{10}-helix of Cbz-[L-Leu-L-Leu-Aib]$_2$-OMe **1**. (C), (D) Right-handed (*P*) -helix of Cbz-[L-Leu-L-Leu-(*S*,*S*)-Ac_5c^{dOM}]$_2$-OMe **3** (molecule *A*). (E) Overlay of molecules *A* and *B* of **3**.

Acknowledgements We thank Prof. I. Azumaya (Tokushima Bunri University) for his invaluable suggestions about CD spectra; and Ms. Y. Sato for her technical assistance. This work was supported by Grants-in-Aid from the Japan Society for the Promotion of Science, Grant-in-Aid from the Tokyo Biochemical Research Foundation, and by the Sasakawa Scientific Research Grant from the Japan Science Society.

References and Notes

1) Karle I. L., Balaram P., *Biochemistry*, **29**, 6747—6756 (1990).
2) Heimgartner H., *Angew. Chem., Int. Ed.*, **30**, 238—264 (1991).
3) Wysong C. L., Yokum T. S., McLaughlin M. L., Hammer R. P., *Chemtech*, **27**, 26—33 (1997).
4) Toniolo C., Crisma M., Formaggio F., Peggion C., Broxterman Q., Kaptein B., *J. Incl. Phenom. Macro. Chem.*, **51**, 121—136 (2005).
5) Branden C., Tooze J., "Introduction to Protein Structure," Garland, New York, 1991, pp. 1—15.
6) Toniolo C., Crisma M., Formaggio F., Valle G., Cavicchioni G., Precigoux G., Aubry A., Kamphuis J., *Biopolymers*, **33**, 1061—1072 (1993).
7) Benedetti E., *Biopolymers (Peptide Science)*, **40**, 3—44 (1996).
8) Tanaka M., *J. Synth. Org. Chem. Jpn.*, **60**, 125—136 (2002).
9) Tanaka M., Nishimura S., Oba M., Demizu Y., Kurihara M., Suemune H., *Chem. Eur. J.*, **9**, 3082—3090 (2003), and references cited therein.
10) Toniolo C., Crisma M., Formaggio F., Peggion C., Broxterman Q. B., Kaptein B., *Biopolymers (Peptide Science)*, **76**, 162—176 (2004).
11) Crisma M., Formaggio F., Moretto A., Toniolo C., *Biopolymers (Peptide Science)*, **84**, 3—12 (2006).
12) Tanaka M., Demizu Y., Doi M., Kurihara M., Suemune H., *Angew. Chem., Int. Ed.*, **43**, 5360—5363 (2004).

13) Isokawa S., Mimura Y., Narita M., *Macromolecules*, **22**, 1280—1284 (1989).
14) Mammi S., Rainaldi M., Bellanda M., Schievano E., Peggion E., Broxterman Q. B., Formaggio F., Crisma M., Toniolo C., *J. Am. Chem. Soc.*, **122**, 11735—11736 (2000).
15) Pengo P., Pasquato L., Moro S., Brigo A., Fogolari F., Broxterman Q. B., Kaptein B., Scrimin P., *Angew. Chem., Int. Ed.*, **42**, 3388—3392 (2003).
16) CCDC-602473, and 602475 contain the supplementary crystallographic data for this paper. These data can be obtained free of charge *via* www.ccdc.cam.ac.uk/conts/retrieving.html (or from the Cambridge Crystallographic Data Centre, 12, Union Road, Cambridge CB2 1EZ, UK; fax: (+44) 1223-336-033; or deposit@ccdc.cam.ac.uk). Crystal data: **1**: $C_{41}H_{68}N_4O_6$, Mr=789.0, space group $P1$, a=10.411, b=11.003, c=11.330 Å, =106.31°, =94.75°, =103.83°, V=1193.8 Å^3, Z=1, T=302 K, (MoK)=0.77 cm^{-1}, 3417 reflections measured, 2950 unique reflections (R_{int}=0.0252) R_1 (I>2)=0.0434, wR_2 (I>2)=0.0870, GOF=1.576. **3**: $2(C_{46}H_{80}N_6O_{13})\cdot CH_4O\cdot H_2O$, Mr=1972.4, space group $P1$, a=12.903, b=14.824, c=16.669 Å, =104.88°, =93.48°, =112.92°, V=2791.8 Å^3, Z=2, T=200 K, (MoK)=0.86 cm^{-1}, 12192 reflections measured, 10971 unique reflections (R_{int}=0.0248) R_1 (I>2)=0.0522, wR_2 (I>2)=0.1427, GOF=1.010.
17) In both peptides **1** and **3**, and sign inversions at the C-terminus are observed. Thus for mean value calculations, the C-terminal residues were omitted.
18) Conformational search calculations were performed with the package of *MacroModel* ver. 8.1 (Schrodinger, Inc.) on SGI workstation. Monte Carlo Multiple Minimum (MCMM) method and AMBER* force field were used for finding the global minimum energy conformation and local ones. As initial structures, extended structure, 3_{10}-helix and -helix structures were used. More than 50000 conformers were optimized. The right-handed (P) -helix of **3** produced by the restricted calculation was a local minimum-energy conformation, which was less stable than the 3_{10}-helical conformation by +9.24 kcal/mol.
19) Francis A. K., Iqbal M., Balaram P., Vijayan M., *J. Chem. Soc., Perkin Trans. 2*, **1982**, 1235—1239 (1982).
20) Tanaka M., Anan K., Demizu Y., Kurihara M., Doi M., Suemune H., *J. Am. Chem. Soc.*, **127**, 11570—11571 (2005).
21) Tanaka M., *Yakugaku Zasshi*, **126**, 931—944 (2006).
22) Tanaka M., *Chem. Pharm. Bull.*, **55**, 349—358 (2007).